Title: Identification of a plant kinase that phosphorylates the bacterial effector AvrPtoB

Running Title: Phosphorylation of the AvrPtoB effector by SnrK2.8

Authors and Affiliations: Lei Lei[1], Danielle M. Stevens[1], Gitta Coaker[1*]

[1]Department of Plant Pathology, University of California, Davis, Davis, CA, USA

*Corresponding author: Gitta Coaker; Email: glcoaker@ucdavis.edu

Abstract

A critical component controlling bacterial virulence is the delivery of pathogen effectors into plant cells during infection. Effectors alter host metabolism and immunity for pathogen benefit. Multiple effectors are phosphorylated by host kinases, and this posttranslational modification is important for their activity. We sought to identify host kinases involved in effector phosphorylation. Multiple effector phosphorylated residues matched the proposed consensus phosphorylation motif of the plant calcium-dependent protein kinase (CDPK) and Snf1-related kinase (SnRK) superfamily. The conserved *Pseudomonas* effector AvrPtoB acts as an E3 ubiquitin ligase and promotes bacterial virulence. We identified a member of the Arabidopsis SnRK family, SnRK2.8, that associated with AvrPtoB in yeast and *in planta*. *SnRK2.8* was required for AvrPtoB virulence functions, including facilitating bacterial colonization, suppression of callose deposition, and targeting the plant defense regulator NPR1 and flagellin receptor FLS2. Mass spectrometry revealed AvrPtoB was phosphorylated at multiple serine residues *in planta,* with S258 phosphorylation reduced in the *snrk2.8* knockout. AvrPtoB phospho-null mutants exhibited compromised virulence functions and were unable to suppress NPR1 accumulation, FLS2 accumulation, or inhibit FLS2-BAK1 complex formation upon flagellin perception. These data identify a conserved plant kinase utilized by a pathogen effector to promote disease.

Introduction

Plants are exposed to diverse pathogens and rely on both passive and active defenses in order to restrict infection. Passive plant defenses include a waxy cuticle, pre-formed antimicrobial compounds, and the cell wall (Gu et al., 2017). Inducible defenses are often triggered by membrane-localized pattern recognition receptors (PRRs) as well as intracellular nucleotide-binding site leucine-rich repeat proteins (NLRs) (Boutrot and Zipfel, 2017; Lolle et al., 2020). Common plant immune responses after active pathogen perception include the production of reactive oxygen species (ROS), callose deposition, activation of mitogen-activated protein kinases, and global transcriptional reprogramming towards defense (Bigeard et al., 2015; Peng et al., 2018).

To colonize their hosts, pathogens rely on the ability to secrete effector proteins. Characterized effectors act to suppress plant immune responses, alter host developmental processes, and affect host metabolism to promote pathogen infection (Toruño et al., 2015). Bacterial pathogens have the most well-characterized effector repertoires. For example, the *Pseudomonas syringae* effectors AvrPto and HopAO1 directly interact with the cytoplasmic domains of the PRRs FLAGELLIN-SENSING 2 (FLS2) and ELONGATION FACTOR-Tu RECEPTOR (EFR), and inhibit PRR kinase activity (Xiang et al., 2008; Macho et al., 2014). Effectors are also capable of manipulating plant hormone processes. The *P. syringae* effector HopX1 and its *Ralstonia solanacearum* homolog RipE1 are cysteine proteases that degrade multiple JASMONATE-ZIM DOMAIN (JAZ) transcriptional repressors to activate jasmonic acid signaling, suppress plant salicylic acid (SA)-mediated defense responses, and open stomatal apertures (Gimenez-Ibanez et al., 2014; Nakano and Mukaihara, 2019). Multiple *Xanthomonas oryzae* pv. *oryzae* transcriptional activator-like effectors, PthXo1, TalC, AvrXa7, PthXo3, and Tal5, induce the expression of sucrose transporter genes *OsSWEET11* or *OsSWEET14*, which could alter metabolism or nutrient acquisition (Streubel et al., 2013; Zhou et al., 2016; Tran et al., 2018). The diverse functions of pathogen effectors make them excellent molecular probes to investigate plant biological processes.

Despite the collective importance of effectors for pathogen virulence, higher-order effector deletions are normally required to observe strong effects. Two *P. syringae* effectors, *AvrPto* and *AvrPtoB*, are conserved in many *P. syringae* pathovars and are collectively required for pathogen

58 virulence and bacterial growth *in planta* (Lin and Martin, 2005). AvrPto and AvrPtoB are
59 partially redundant. For example, in *Arabidopsis* both AvrPto and AvrPtoB associate with the
60 flagellin receptor FLS2 and interfere with downstream defense signaling (Shan et al., 2008). In
61 tomato, both AvrPto and AvrPtoB interact with the Pto kinase, leading to recognition by the
62 NLR Prf (Kim et al., 2002; Xiao et al., 2007a). However, compared with AvrPto, AvrPtoB has a
63 more complex structure. The N-terminus of AvrPtoB comprises multiple target-binding domains
64 and its C-terminus is a U-box type E3 ubiquitin ligase, which mediates the degradation of target
65 proteins through the host proteasome (Abramovitch et al., 2006). AvrPtoB associates with both
66 FLS2 and its co-receptor BAK1, disrupts flagellin 22 (flg22) induced FLS2-BAK1 complex
67 formation, and mediates the degradation of FLS2 (Göhre et al., 2008; Shan et al., 2008). NPR1
68 (NON-EXPRESSER OF PR GENES 1) is an essential regulator of salicylic acid (SA)-
69 dependent defense gene expression (Withers and Dong, 2016; Chen et al., 2019). AvrPtoB
70 associates with NPR1 and mediates the degradation of NPR1 in the presence of SA (Chen et al.,
71 2017). In addition, AvrPtoB also targets the protein kinase Fen, the chitin receptor CERK1, and
72 the exocyst complex protein EXO70B1 (Rosebrock et al., 2007; Gimenez-Ibanez et al., 2009;
73 Wang et al., 2019). AvrPtoB's diverse targets demonstrate its prominent role in *P. syringae*
74 infection.

75 Although effectors are produced in the pathogen, they are activated upon delivery and function
76 inside their host. For instance, the *P. syringae* effector protease AvrRpt2 requires the plant
77 protein folding catalyst and chaperone cyclophilin for activation (Coaker et al., 2005). Several
78 pathogen effectors target plant nuclei and rely upon host importin-α for nuclear translocation,
79 including the *Xanthomonas* bacterial effector AvrBs3 and the *Hyaloperonospora* oomycete
80 effector HaRxL106 (Szurek et al., 2001; Bai et al., 2009; Schornack et al., 2013; Wirthmueller et
81 al., 2014). Collectively, these studies highlight diverse plant proteins that are required for
82 mediating the activation, localization, and virulence activities of pathogen effectors.

83 Pathogen effectors also rely upon host phosphorylation to promote their virulence activity (Xing
84 et al., 2002; Bhattacharjee et al., 2015). Truncated AvrPtoB$_{1\text{-}307}$ is phosphorylated in different
85 plants including tomato, *Nicotiana benthamiana*, and *Arabidopsis thaliana*. The substitution of
86 the serine 258 phosphorylated residue on AvrPtoB$_{1\text{-}307}$ to alanine results in significantly
87 attenuated virulence on susceptible tomato genotypes (Xiao et al., 2007a). The *P. syringae*

effectors AvrPto, AvrB, and HopQ1 as well as the *Rhizobium* effectors NopL, NopP, and the cyst nematode effector 10A07 also target and recruit host kinases to promote their virulence (Desveaux et al., 2007; Li et al., 2013; Hewezi et al., 2015; Tahir et al., 2019). With the exception of the nematode effector 10A07, the host kinases utilized by these pathogen effectors remain unknown.

In this study, we investigated the identity of the host kinase that phosphorylates AvrPtoB. *SnRK2.8*, a member of sucrose non-fermenting-1(SNF1)-related kinase (SnRK) family in *Arabidopsis*, is involved in NPR1 mediated systemic acquired resistance and several abiotic stress signaling pathways (Umezawa et al., 2004; Fujii et al., 2011; Lee et al., 2015). Here, we show that SnRK2.8 interacts with and phosphorylates AvrPtoB on three conserved serine residues *in planta*. AvrPtoB requires these three phosphorylated residues as well as *SnRK2.8* for virulence. The *snrk2.8* knockout and AvrPtoB phospho-null mutations blocked AvrPtoB virulence activities, including the ability to inhibit NPR1 and FLS2 protein accumulation as well as disrupt ligand-induced FLS2-BAK1 complex formation. Taken together, our results identify a conserved plant kinase recruited by a core *P. syringae* effector to promote virulence.

Results

The *Pseudomonas syringae* effector AvrPtoB interacts with the plant kinase SnRK2.8.

To investigate which plant kinases may be capable of phosphorylating pathogen effectors, we analyzed the sequence of previously identified effector phosphorylation sites (Supplemental Table 1). Interestingly, most effector phosphorylation sites, including AvrPtoB's phosphorylated residues, matched the proposed consensus phosphorylation motif of the sucrose non-fermenting-1 (SNF1)-related kinases (SnRKs) and calcium-dependent protein kinases (CDPKs) (R-$X_{(2-3)}$-S/T or S/T- $X_{(1-2)}$-R) (Klimecka and Muszyńska, 2007; Vlad et al., 2008) (Supplemental Figure 1). SnRK-CDPK family is conserved in plants and involved in a range of metabolic and stress signaling pathways, such as carbohydrate biosynthesis, abscisic acid (ABA)-induced signaling, salinity tolerance, cold stress, and response to pathogen infection (Coello et al., 2011; Hulsmans et al., 2016). Transcriptional profiling data from the BAR Expression Angler revealed that multiple SnRK members are induced upon activation of plant defense, including application of SA, the immunogenic flagellin epitope flg22, or infection with the *P. syringae* type III secretion mutant △hrcC (Boudsocq et al., 2010; Gao et al., 2013) (Figure 1A).

118 Next, we analyzed the ability of diverse SnRK/CDPK members to interact with AvrPtoB by
119 yeast two-hybrid. The plant protein kinase Pto was used as a positive control (Figure 1B). We
120 analyzed 32 SnRKs for the ability to interact with AvrPtoB by yeast-two hybrid (Supplemental
121 Figure 2). SnRK1.1, SnRK2.6, and SnRK2.8 specifically interacted with AvrPtoB (Figure 1B
122 and C). Some CDPK subgroup I members are involved in flg22 signaling and NLR immune
123 responses, so we cloned these CDPK members (CPK2, 4, 5, 6, 11 and 26) and three other
124 members from subgroups which can induce defense gene expression after flg22 application
125 (Boudsocq et al., 2010; Gao et al., 2013). Auto-active CDPKs were generated by deleting their
126 C-terminal Ca^{2+} regulatory and auto-inhibitory domains (CPKs△C) for yeast-two hybrid
127 screening (Klimecka and Muszyńska, 2007). CPK4△C and CPK5△C specifically interacted
128 with AvrPtoB (Figure 1B, C and Supplemental Figure 2). The expression of AvrPtoB, SnRKs,
129 and CDPKs in yeast were verified by western blotting (Supplemental Figure 3). AvrPtoB,
130 SnRKs, and CPKs△C did not induce auto-activity in yeast (Figure 1C).

131 To validate the association of AvrPtoB with the SnRK/ CDPK members identified by yeast-two
132 hybrid, we performed co-immunoprecipitation (Co-IP) in *Nicotiana benthamiana*. To enhance
133 the transient interaction between kinase and substrate, kinase-dead variants (KD) of five SnRK/
134 CPK△C members were generated by mutating the lysine residue (K) in their ATP binding
135 pocket to alanine (A). *AvrPtoB-GFP* under the control of a dexamethasone (Dex)-inducible
136 promoter was co-expressed with each *35S:: SnRKs-KD-HA/CPKs△C-KD-HA* in *N. benthamiana*
137 and immunoprecipitation (IP) was performed with anti-GFP agarose beads. Immunoblotting
138 results demonstrated that SnRK1.1, SnRK2.6, CPK4△CA, and CPK5△C weakly associated
139 with AvrPtoB (Figure 1D and E). Only SnRK2.8 strongly associated with AvrPtoB (Figure 1D
140 and E). The strong association of SnRK2.8 with AvrPtoB in yeast and *in planta* suggests that
141 SnRK2.8 may play an important role in AvrPtoB phosphorylation.

142 **AvrPtoB is phosphorylated by SnRK2.8.**

143 To investigate whether SnRK2.8 phosphorylates AvrPtoB, we tested the phosphorylation by
144 SnRK2.8 *in vitro*. Recombinant GST-AvrPtoB and GST-SnRK2.8 proteins were purified from *E.*
145 *coli,* subjected to kinase activity assays, and protein phosphorylation was detected by
146 immunoblot with antibodies recognizing pSer/pThr residues. Purified SnRK2.8 is an active
147 kinase and exhibits strong auto-phosphorylation (Figure 2A). No phosphorylation was detected

148 in the sample only containing purified AvrPtoB. However, after incubation with SnRK2.8,
149 AvrPtoB phosphorylation was detected in SnRK2.8 dose-dependent manner (Figure 2A). These
150 results indicate that SnRK2.8 is able to phosphorylate AvrPtoB *in vitro*.

151 Next, we investigated AvrPtoB phosphorylation *in vivo*. AvrPtoB-GFP was expressed in
152 *Arabidopsis* Col-0 protoplasts, enriched by anti-GFP IP, and samples were subjected to trypsin
153 digestion and mass spectrometry analyses (LC-MS/MS). Five phosphorylated AvrPtoB residues
154 (T111, S205, S210, S217, and S258) were identified by LC-MS/MS (Figure 2B). Previously,
155 AvrPtoB was demonstrated to be phosphorylated at S258 in tomato, indicating that
156 phosphorylation of this residue is conserved across diverse plant species (Xiao et al., 2007b).
157 Aside from T111, all other phosphorylated residues map to specific domains required for binding
158 the target proteins NPR1 (S205, S210, S217, and S258) and BAK1 (S258) (Figure 2C). The
159 region surrounding S258 matches the proposed consensus phosphorylation motif of the
160 SnRKs/CDPKs (Supplemental Table 1).

161 To determine the importance of SnRK2.8 for AvrPtoB phosphorylation *in planta,* AvrPtoB-GFP
162 was expressed in *Arabidopsis* protoplasts from both wild-type Col-0 and the *snrk2.8* knockout.
163 AvrPtoB-GFP was then immunoprecipitated after transfection, subjected to trypsin digestion and
164 LC-MS/MS using parallel reaction monitoring (PRM). Using PRM, we were able to detect
165 phosphorylation of the five previously identified AvrPtoB residues. The phosphorylation ratios
166 (phosphorylated/nonphosphorylated peptides) of T111 and S217 were similar between Col-0 and
167 *snrk2.8* (Supplemental Figure 4A and B). However, the phosphorylation ratios of the other three
168 residues were lower in *snrk2.8* compared to Col-0. Phosphorylation of S258 was significantly
169 reduced by over 90% in *snrk2.8* and phosphorylation of S205 and S210 were reduced by ～50%
170 (Figure 2D). Notably, S205, S210, and S258 are highly conserved as either S or T residues
171 across 27 *Pseudomonas* AvrPtoB homologs (Supplemental Figure 5). Taken together, these
172 results indicate that SnRK2.8 can directly phosphorylate AvrPtoB *in vitro* and *in vivo.*

173 ***SnRK2.8* is required for AvrPtoB virulence**

174 AvrPtoB's phosphorylated residues are located within regions known to bind to plant targets,
175 which led us to investigate whether *SnRK2.8* is required for AvrPtoB virulence (Figure 2C).
176 Since AvrPto and AvrPtoB are redundant with respect to virulence, a *Pseudomonas syringae* pv.

177 *tomato* DC3000 *avrPto* and *avrPtoB* double knockout strain was used (Lin et al., 2005).
178 DC3000Δ*avrPto*Δ*avrPtoB* (DC3000 -/-) was transformed with a plasmid expressing *AvrPtoB* or
179 the empty vector (EV) control. Col-0 and *snrk2.8* plants were inoculated with DC3000 and
180 DC3000 -/- strain variants by syringe infiltration. Four days post-inoculation DC3000 caused
181 severe disease symptoms, while DC3000 -/- EV caused weak disease symptoms on both Col-0
182 and *snrk2.8* (Figure 3A). DC3000 -/- carrying *AvrPtoB* caused much more severe symptoms
183 compared to DC3000 -/- carrying EV on Col-0, but not the *snrk2.8* knockout (Figure 3A).
184 Consistent with the disease symptoms, the bacterial titer of DC3000 -/- *AvrPtoB* was
185 significantly higher than that of DC3000 -/- EV in Col-0, but not in the *snrk2.*8 knockout (Figure
186 3B). These results indicate that *SnRK2.8* is required for AvrPtoB virulence in *Arabidopsis*.

187 AvrPtoB suppresses plant defense triggered by PAMP recognition including the deposition of
188 callose, a β-1–3 linked glucan polymer, that is defense induced and acts as a structural barrier
189 (Torres et al., 2006). To investigate the impact of *SnRK2.8* on AvrPtoB virulence, we examined
190 callose deposition after inoculation with DC3000 -/- carrying EV or *AvrPtoB*. DC3000 -/-
191 carrying EV elicited strong callose deposition in both Col-0 and *snrk2.8* (Figure 3C and D). As
192 expected, DC3000 -/- carrying *AvrPtoB* did not elicit strong callose deposition in Col-0.
193 However, *AvrPtoB* was unable to suppress callose deposition in the *snrk2.8* knockout (Figure 3C
194 and D). These data indicate that AvrPtoB requires the plant kinase *SnRK2.8* for suppressing
195 callose deposition in *Arabidopsis*.

196 **Phosphorylated AvrPtoB serine residues are required for virulence**

197 To test the functional relevance of AvrPtoB phosphorylation, we analyzed the virulence of
198 AvrPtoB phospho-null mutants. We focused on S205, S210 and S258 due to their decrease in
199 phosphorylation in the *snrk2.8* knockout (Figure 2D). These serine residues were replaced by
200 alanine to create single and triple phospho-null mutations. Previous research demonstrated that
201 the alanine substitution of S258 resulted in a loss of virulence of $AvrPtoB_{1–307}$ on the susceptible
202 tomato genotype Rio Grande 76S (lacking the resistance gene Prf) (Xiao et al., 2007b). We first
203 tested the ability of full-length $AvrPtoB_{S258A}$ to promote bacterial growth on Rio Grande 76S and
204 *Arabidopsis* Col-0. The DC3000 -/- strain expressing $AvrPtoB_{S258A}$ was able to increase bacterial
205 growth in both tomato and *Arabidopsis,* but not to the same extent as wild-type *AvrPtoB*
206 (Supplemental figure 6A and B). In contrast, the DC3000 -/- strain expressing the 1-307

207 truncation of *AvrPtoB*$_{S258A}$ was unable to increase bacterial growth in both tomato and
208 *Arabidopsis* (Supplemental Figure 6A and B). These results indicate that the phosphorylation of
209 S258 is important, but not sufficient, for the virulence of full-length AvrPtoB.

210 Next, we tested the virulence of the phospho-null mutant AvrPtoB$_{S205AS210A258A}$ compared to
211 wild-type AvrPtoB and AvrPtoB$_{S258A}$. *Arabidopsis* Col-0 was syringe infiltrated with DC3000 -/-
212 carrying EV, *AvrPtoB, AvrPtoB*$_{S258A}$, and *AvrPtoB*$_{S205AS210A258A}$. Disease symptoms, bacterial
213 titers, callose deposition were analyzed. As expected, infection with DC3000 -/- carrying
214 *AvrPtoB* resulted in leaf disease symptoms, increased bacterial growth, and suppression of
215 callose deposition compared to EV (Figure 4). Infection with DC3000 -/- *AvrPtoB*$_{S258A}$ resulted
216 in an intermediate phenotype, with slight disease symptoms, a partial increase in bacterial growth
217 compared to EV, and partial suppression of callose compared to EV (Figure 4). However,
218 DC3000 -/- carrying *AvrPtoB*$_{S205AS210A258A}$ was unable to induce disease symptoms, grew to the
219 same level as the EV control, and was unable to suppress callose deposition (Figure 4). Western
220 blot analyses demonstrated that all AvrPtoB variants were equally expressed in DC3000 -/-
221 (Supplemental Figure 6C). Collectively, these results demonstrate that the combined
222 phosphorylation of S205, S210, and S258 play a critical role in AvrPtoB virulence.

223 **AvrPtoB-mediated inhibition of NPR1 accumulation requires the plant kinase SnRK2.8**

224 AvrPtoB associates with and ubiquitinates NPR1 in the presence of SA (Chen et al., 2017). To
225 further investigate the relevance of SnRK2.8 for promoting AvrPtoB virulence, we examined
226 AvrPtoB-mediated inhibition of NPR1 accumulation in Col-0 and *snrk2.8*. Both Col-0 and
227 *snrk2.8* were pretreated with 0.5mM SA for 6 hours and then syringe inoculated with DC3000 -/-
228 EV and DC3000 -/- *AvrPtoB*. NPR1 accumulation was detected by anti-NPR1 immunoblotting.
229 Infection with DC3000 -/- EV induced high accumulation of NPR1 in both Col-0 and *snrk2.8*
230 (Figure 5A and B). However, infection with DC3000 -/- *AvrPtoB* inhibited NPR1 accumulation
231 in Col-0, but not in the *snrk2.8* knockout, indicating that *SnRK2.8* is required for AvrPtoB-
232 mediated inhibition of NPR1 accumulation (Figure 5A and B).

233 Next, the importance of AvrPtoB phosphorylated residues for inhibition of NPR1 accumulation
234 was examined. We co-expressed *35S::NPR1-HA* and DEX inducible *AvrPtoB-FLAG, AvrPtoB*
235 phospho-null, and *AvrPtoB* phospho-mimetic mutants in *N. benthamiana*. Wild-type AvrPtoB,
236 AvrPtoB$_{S258D}$, and AvrPtoB$_{S205DS210DS258D}$ significantly decreased NPR1 accumulation compared

237 to the EV control (Figure 5C and D). Both AvrPtoB$_{S258D}$ and AvrPtoB$_{S205DS210DS258D}$ were able to
238 strongly suppress NPR1 accumulation, indicating that mimicking phosphorylation also promotes
239 virulence of AvrPtoB (Figure 5C and D). AvrPtoB$_{S258A}$ was still able to suppress the
240 accumulation of NPR1, indicating that the phosphorylation of serine 258 is not sufficient for this
241 function of AvrPtoB (Figure 5C and D). In contrast, AvrPtoB$_{S205AS210A258A}$ was unable to
242 suppress NPR1 accumulation (Figure 5C and D). Collectively, these results show that AvrPtoB-
243 mediated inhibition of NPR1 accumulation requires the plant kinase SnRK2.8 and the SnRK2.8-
244 mediated phosphorylated residues.

245 **AvrPtoB-mediated inhibition of FLS2 accumulation and FLS2-BAK1 complex formation**
246 **requires the plant kinase SnRK2.8**

247 The flagellin receptor FLS2 is another host target of AvrPtoB (Gómez-Gómez and Boller, 2000;
248 Lu et al., 2011). AvrPtoB directly associates with FLS2 and ubiquitinates FLS2 (Göhre et al.,
249 2008). To investigate the relevance of SnRK2.8 with AvrPtoB-mediated inhibition of FLS2
250 accumulation, we compared FLS2 accumulation after infection with DC3000 -/- carrying EV or
251 *AvrPtoB* in different genetic backgrounds. Col-0 and the *snrk2.8* knockout were syringe
252 inoculated and FLS2 accumulation was detected by anti-FLS2 immunoblotting. FLS2
253 accumulation was enhanced after infection with DC3000 -/- EV in both Col-0 and *snrk2.8*
254 (Figure 6A and B). In contrast, *AvrPtoB* was able to suppress FLS2 accumulation in Col-0 but
255 not in the *snrk2.8* knockout, which demonstrates that *SnRK2.8* is required for AvrPtoB-mediated
256 suppression of FLS2 accumulation (Figure 6A and B).

257 To test if AvrPtoB phosphorylated residues are required for inhibition of FLS2 accumulation, we
258 co-expressed *35S::FLS2-GFP* and DEX inducible *AvrPtoB-FLAG*, *AvrPtoB* phospho-null, and
259 *AvrPtoB* phospho-mimetic mutants in *N. benthamiana*. Wild-type AvrPtoB, AvrPtoB$_{S258D}$, and
260 AvrPtoB$_{S205DS210DS258D}$ significantly decreased FLS2 accumulation compared to the EV control
261 (Figure 6C and D). AvrPtoB$_{S258A}$ was still able to decrease the accumulation of FLS2, indicating
262 that the phosphorylation of serine 258 is not sufficient for this AvrPtoB function (Figure 6C and
263 D). In contrast, the phospho-null mutant AvrPtoB$_{S205AS210AS258A}$ was unable to suppress FLS2
264 accumulation (Figure 6C and D). Collectively, these results demonstrate that AvrPtoB
265 phosphorylated residues and the plant kinase SnRK2.8 are required for inhibition of FLS2
266 accumulation.

267 FLS2-mediated recognition of flg22 induces the formation of an FLS2-BAK1 complex, which is
268 required for downstream immune signaling (Chinchilla et al., 2007; Shan et al., 2008). We
269 investigated the importance of AvrPtoB phosphorylated residues for disrupting FLS2-BAK1
270 complex formation. We examined flg22-induced FLS2-BAK1 association in the presence of
271 AvrPtoB and AvrPtoB phospho-null mutants after transient expression in *N. benthamiana*. As
272 shown in Figure 6E, wild-type AvrPtoB effectively diminished FLS2-BAK1 association in the
273 presence of flg22, but AvrPtoB$_{S258A}$ and AvrPtoB$_{S205AS210AS258A}$ were unable to suppress FLS2-
274 BAK1 complex formation. These results suggest that phosphorylation of S258 is required and
275 sufficient for disrupting FLS2-BAK1 complex formation.

276 **Discussion**

277 Post-translational modification (PTM) is a rapid and specific protein regulation mechanism that
278 plays important roles in plant growth, development, and disease resistance (Withers and Dong,
279 2017). Recent comprehensive proteome analyses in Arabidopsis reveal that 47% of the identified
280 proteins are phosphorylated under specific conditions(Withers and Dong, 2017; Mergner et al.,
281 2020). Many pathogen effectors require PTM *in planta* for their virulence activity. Effectors
282 from the bacterial pathogens *Pseudomonas syringae*, *Xanthomonas*, and *Rhizobium* are
283 phosphorylated in plants (Li et al., 2013; Kim et al., 2014; Tahir et al., 2019). The
284 phosphorylation of effectors by plant kinases, in many instances, enhances their virulence-
285 promoting activity (Tahir et al., 2019). However, the host kinases involved in effector
286 phosphorylation are largely unknown. Our study reveals that the AvrPtoB is phosphorylated on
287 five serine/threonine residues, three of which (S205, S210, and S258) are required for AvrPtoB
288 virulence in *Arabidopsis* and conserved across *P. syringae* AvrPtoB. One SnRK family member,
289 SnRK2.8, interacts with AvrPtoB, is primarily responsible for phosphorylating AvrPtoB, and is
290 required for AvrPtoB virulence promoting activities.

291 Sucrose non-fermenting-1 (SNF1)-related protein kinases (SnRKs) are the plant homologs of
292 SNF1 kinase in yeast and AMP-activated protein kinase (AMPK) in mammals, which are key
293 regulators of carbon metabolism and energy status (Coello et al., 2011; Hardie et al., 2012). The
294 plant SnRK family can be subdivided into three subfamilies: SnRK1, SnRK2, and SnRK3. The
295 SnRK2 subfamily members have diverged from Snf1 and AMPK and are plant specific. SnRKs
296 act as metabolic sensors, integrating multiple developmental processes and very diverse stress

297 conditions including pathogen infection (Halford and Hey, 2009; Hulsmans et al., 2016) An
298 increasing number of studies show the key roles of SnRKs in plant responses to different types of
299 pathogens. Tomato SnRK1 phosphorylates the pathogenic protein βC1 of the tomato yellow leaf
300 curl virus to limit viral infection (Shen et al., 2011). Tomato SnRK1 is also involved in cell death
301 elicited by *Xanthomonas* effectors and may be related to Adi3-mediated suppression of cell death
302 (Szczesny et al., 2010; Avila et al., 2012).

303 SnRK2.8, an *Arabidopsis* SnRK2 member, is transcriptionally induced by infection with *P.*
304 *syringae* DC3000 and mediates SA induced systemic acquired resistance (Lee et al., 2015).
305 SnRK2.8 phosphorylates NPR1 in the cytoplasm and mediates the nuclear import of NPR1 (Lee
306 et al., 2015). Since both SnRK2.8 and AvrPtoB associate with NPR1, we assume these two
307 proteins are likely in close contact with one another. In the *snrk2.8* knockout, the
308 phosphorylation of S258 is reduced by over 90% and the phosphorylation of S205 and S210 is
309 reduced by ~50%. These results indicate that SnRK2.8 is one of the main kinases involved in
310 AvrPtoB phosphorylation. However, since some phosphorylation of S205/S210/S258 remain in
311 the *snrk2.8* knockout and *SnRK2.8* does not influence phosphorylation of T111 and S217 *in*
312 *planta*, other kinases are also involved phosphorylating AvrPtoB. AvrPtoB weakly associates
313 with SnRK1.1, SnRK2.6 and another two CDPK members in *planta*. These kinases may also be
314 capable of AvrPtoB phosphorylation.

315 Previously, only one kinase has been identified that is capable of phosphorylating a plant
316 pathogen effector. The cyst nematode effector 10A07 interacts with an *Arabidopsis* autophagy
317 related (Atg) 1 kinase, Atg1C, *in planta* (Hewezi et al., 2015). Atg1C phosphorylates 10A07 on
318 two serine residues, which are required for nuclear localization of this effector. An inactive
319 variant of Atg1C reduced the plant susceptibility to cyst nematode (Hewezi et al., 2015).
320 Similarly, AvrPtoB virulence promoting activities are blocked in the *snrk2.8* knockout and
321 SnRK2.8 phosphorylated residues on AvrPtoB are required for effector function. Both SnRKs
322 and Atg kinases are widely conserved among eukaryotes and are involved in plant immune
323 responses (Hayward et al., 2009; Coello et al., 2011). However, these kinases could be a double-
324 edged sword as they are also exploited by pathogen effectors during infection.

325 Phosphorylation can impact protein-protein interactions by creating an intricate binding surface
326 (Tarrant and Cole, 2009). Effectors from human pathogens, including the *E. coli* effector Tir

327 (Translocated intimin receptor) and *Helicobacter pylori* effector CagA (Caytotoxin-associated
328 antigen A) are subjected to host phosphorylation. Phosphorylation of Tir and CagA are required
329 for the binding of host adaptor proteins for bacterial adhesion (Nougayrede et al., 2003; Higashi
330 et al., 2004). The plant pathogen effectors HopQ1, XopN, and XopE2 are phosphorylated in
331 plants, which results in their associations with host 14-3-3 proteins and phosphorylated residues
332 are required for effector virulence (Taylor et al., 2012; Li et al., 2013; Dubrow et al., 2018). In
333 our study, the phosphorylation of AvrPtoB is required for the effector-mediated inhibition of
334 NPR1/FLS2 accumulation and FLS2-BAK1 complex formation. Three critical AvrPtoB
335 phosphorylated residues are not present in the AvrPtoB E3 ligase domain, so they should not
336 directly affect the AvrPtoB ubiquitination activity. Thus, the phosphorylation of AvrPtoB may be
337 required for the interactions with its targets. S258 is located in both the NPR1 and BAK1 binding
338 domains of AvrPtoB, while S205 and S210 are present in the NPR1 binding domain. The single
339 phospho-null S258A mutant was still able to inhibit NPR1/FLS2 accumulation. However, the
340 triple phospho-null mutant completely lost these functions, indicating that the phosphorylation of
341 S205 and S210 is required for AvrPtoB-mediated target degradation (Figure 5C, D and Figure
342 6C, D). However, the S258A was unable to disrupt FLS2-BAK1 complex formation. These data
343 are consistent with previous observations that AvrPtoB is a multifunctional protein with different
344 interfaces involved in interacting with diverse host proteins (Martin, 2011).

345 Despite the importance of effector phosphorylation, the plant kinases involved remain largely
346 elusive. Here, we identified a member of the SnRK-CDPK family, SnRK2.8, whose
347 phosphorylation of the conserved bacterial effector AvrPtoB promotes effector virulence
348 activities. The SnRK-CDPK family is conserved in plants and most reported effectors
349 phosphorylated residues are consistent with the SnRK-CDPK phosphorylation site preferences.
350 Thus, we hypothesize that different SnRKs and CPDKs may be involved in phosphorylation of
351 diverse effector proteins. Future investigation of the role of SnRK-CDPKs in phosphorylation of
352 diverse pathogen effectors will provide a more comprehensive understanding of how pathogen
353 effectors exploit their hosts to facilitate disease development.

354

355

356 **Methods**

357 **Plant material and growth conditions**

358 *Arabidopsis thaliana* seeds were stratified for two days at 4°C in the dark before sowing. Plants
359 were grown in a controlled environmental chamber at 23°C and 70% relative humidity with a 10-
360 hr-light /14-hr-dark photoperiod (100 μM m^{-2} s^{-1}). Four-to-five-week old plants were used for all
361 experiments. A confirmed *snrk2.8* knockout T-DNA insertion line (SALK_073395) in the
362 Columbia (Col-0) background was obtained from the *Arabidopsis* Biological Resource Center
363 (ABRC) (Shin et al., 2007).

364 *N. benthamiana* was grown in a growth chamber at 26°C with a 16-hr-light/8-hr-dark
365 photoperiod (180 μM m^{-2} s^{-1}). Three-to-four-week old plants were used for Agrobacterium-
366 mediated transient protein expression.

367 **Yeast two-hybrid screen**

368 The GAL4 based Matchmaker yeast two-hybrid system was used for the AvrPtoB-kinase
369 interaction screen (Clonetech). *AvrPtoB* and a *mCherry* negative control were cloned into the
370 pGADT7 vector fused to the GAL4 activation domain and HA tag. *Arabidopsis SnRK*s and
371 *CDPKs* were cloned into the pGBKT7 vector, which contains the GAL4 DNA binding domain
372 and N-terminal Myc epitope tag. In order to detect interactions with CDPKs, their C-terminal
373 Ca^{2+} regulatory and auto-inhibitory domains were removed prior to clone into the pGBKT7
374 vector. The pGADT7-*AvrPtoB* and pGADT7-*mCherry* plasmids were separately co-transformed
375 with each pGBKT7-*SnRK/CPKΔC* plasmid into the yeast strain AH109, colonies were selected
376 on SD -Leu/-Trp dropout media and tested for interactions on SD -Leu/-Trp/-His dropout media
377 containing X-α-Gal. Yeast transformation and media preparation were performed per
378 manufacturer instructions (Clontech). To confirm protein expression, yeast proteins were
379 extracted as described previously and subjected to anti-HA HRP (Roche #12013819001;
380 1:2,000) and anti-Myc (Clontech #631206; 1: 2,000) immunoblotting (Zhang et al., 2011).
381 Primers used in all experiments are listed in Table S2.

382

383

384 **Phylogeny and expression of *SnRKs***

385 A total of 38 *Arabidopsis* SnRK protein sequences were obtained from the *Arabidopsis*
386 information resource (TAIR, http://*Arabidopsis*.org). Multiple sequence alignments were
387 performed with MEGA X: Molecular Evolutionary Genetics Analysis across computing
388 platforms (Kumar et al., 2018). The phylogeny was determined by maximum likelihood method
389 (1000 bootstrap replicates). Data of *SnRK* transcriptional expression in leaves were obtained
390 from BAR Expression Angler (Austin et al., 2016).

391 **Co-immunoprecipitation assays**

392 To confirm the association between AvrPtoB and SnRK/CDPKs *in planta*, kinase dead variants
393 were generated and tested for their ability to associate with wild-type AvrPtoB after transient
394 expression in *N. benthamiana. SnRK1.1-KD* (K71A), *SnRK2.6-KD* (K50A), *SnRK2.8-KD*
395 (K33A), *CPK4ΔC-KD* (K54A) and *CPK5ΔC-KD* (K126A) kinase dead variants were generated
396 by PCR-based site-directed mutagenesis and fused with a C-terminal HA tag in the binary vector
397 pGWB414 (NAKAGAWA et al., 2007). Primers are listed in Table S2. *AvrPtoB* fused with a C-
398 terminal GFP tag was cloned into the dexamethasone (Dex)-inducible binary vector pTA7001
399 (Gu and Innes, 2011). Binary vectors were transformed into *Agrobacterium tumefaciens*
400 GV3101. *Agrobacterium* suspensions were co-infiltrated into *N. benthamiana* leaves at an
401 OD600 = 0.4 for AvrPtoB and an OD600 = 0.6 for each kinase. Twenty-four hours post-
402 inoculation, 15 μM DEX and 0.01% Silwet L-77 were sprayed to induce the expression of
403 AvrPtoB-GFP. Two grams of leaf tissue per sample were collected three hours post-DEX
404 application.

405 For immunoprecipitations, *N. benthamiana* leaf tissues were ground in liquid nitrogen and re-
406 suspended in 2 mL IP buffer (50mM Tris-HCL ph7.5, 150mM NaCl, 0.1% Triton, 0.2% NP-40,
407 1× complete protease inhibitor (Thermo Fisher Scientific #A32963) and 1× phosphatase inhibitor
408 (Thermo Fisher Scientific #A32957), 1mM DTT, 40uM MG132, 0.5% PVP). Samples were
409 centrifuged at 14,000 rpm for 15 min and filtered to remove debris using a poly-prep
410 chromatography column (10mL, Bio-Rad). The supernatant was incubated with 25 μL of anti-
411 GFP agarose beads at 4°C for 1.5 hr. Beads were washed once with IP buffer by centrifuging at
412 3000 rpm for two min and twice by filtration through a pierce centrifuge column (0.8 mL, Bio-
413 Rad). Proteins were eluted from the beads by boiling in 2× Laemmli buffer for five min. Proteins

414 were separated by SDS-PAGE and immunoblotted with anti-HA HRP (Roche #12013819001;
415 1:2,000) and anti-GFP HRP (Miltenyi Biotec #130-091-833; 1:3,000).

416 To test the ability of AvrPtoB phosphorylation mutants to disrupt FLS2-BAK1 complex
417 formation, *AvrPtoB* phospho-null mutants (S258A and S205AS210AS258A) were generated by
418 PCR-based site-directed mutagenesis. Primers are listed in Table S2. *AvrPtoB* variants were
419 fused with C-terminal 3× FLAG tag in binary vector pTA7001, and *FLS2* and *BAK1* were
420 separately fused with C-terminal GFP tag and HA tag in binary vector pEarleyGate 103 and
421 pGWB14 (Earley et al., 2006; NAKAGAWA et al., 2007). The binary vectors were transformed
422 into *Agrobacterium tumefaciens* GV3101. *FLS2*, *BAK1*, and *AvrPtoB* variants *Agrobacterium*
423 suspensions were co-infiltrated into *N. benthamiana* leaves, 15 μM DEX and 0.01% Silwet L-77
424 were sprayed to induce the expression of AvrPtoB at 24 hpi for three hours, two grams of leaf
425 tissue for each sample were collected after 15 min treatment with 5 mM $MgCl_2$ or 10 μM flg22.
426 Immunoprecipitation was performed as described above.

427 **Recombinant protein purification**

428 *AvrPtoB* and *SnRK2.8* were cloned in *E.coli* expression vector pDEST15 (Invitrogen) fused with
429 N-terminal GST tag, the constructs were transformed into *E.coli* BL21 (DE3). 200 mL of *E.coli*
430 culture was grown at 28 ℃ until OD600 = 0.5. Protein expression was induced with 0.5mM
431 IPTG at 16 ℃ for 12 hr. Cells were harvested by centrifuging at 5000 g 4 ℃ for 10 min and
432 washed once with buffer A (0.1 M Tris-HCl pH 7.5, 150 mM NaCl, 1 mM PMSF, 1 × CPI, 10
433 mM DTT and 10 uM MG132). Cell pellets were resuspended in 3 mL of buffer A with 15
434 μg/mL lysozyme and incubated on ice for 30 min. Total protein was released by sonication and
435 incubated with Glutathione Sepharose 4B (GE Healthcare #GE17-0756-01) at 4 ℃ for one hour.
436 Agarose beads were washed three times with buffer A by centrifuging at 5000 g for 5 min.
437 Proteins were eluted by incubating with buffer B (50 mM Tris-HCl pH8, 10 mM reduced
438 Glutathione) for 10 min at room temperature (RT).

439 **Kinase activity assay**

440 An *in vitro* kinase activity assay was performed with recombinant proteins, 3 μg of GST-
441 AvrPtoB and 0.3-1 μg GST-SnRK2.8 were mixed in kinase buffer (20 mM Tris-HCl pH7.5, 10
442 mM $MgCl_2$, 1 mM $CaCl_2$, 100 μM ATP, 1 mM DTT). The kinase reaction was performed at

443 30 °C for 30 min and stopped by 3 × Laemmli buffer. Protein samples were separated in SDS-
444 PAGE and immunoblotted with anti-pSer/Thr antibody (Sigma #P3430; 1:1000) and anti-GST
445 antibody (Sigma; 1: 3000).

446 **Phosphorylation site identification and quantification**

447 To identify AvrPtoB phosphorylation sites *in vivo*, *AvrPtoB-YFP* in the pBluescript vector was
448 transiently expressed in Col-0 and *snrk2.8* protoplasts, protoplast preparation and transient
449 transformation were performed as previously described (Yoo et al., 2007). One mL of
450 protoplasts were transfected with 100 µg of plasmid and collected after 9 hr. Proteins were
451 released in IP buffer (without 0.5% PVP) and subject to GFP-IP as described above. Protein
452 peptides were generated by in-solution trypsin digest as previously described and subjected to
453 LC-MS/MS run by Orbitrap Fusion Lumos mass spectrometer (Thermo Fisher Scientific) at the
454 UC Davis Proteomics Core (Minkoff et al., 2013). LC-MS/MS data were analyzed in MaxQuant
455 (Tyanova et al., 2016).

456 To quantify the phosphorylated peptides, an inclusion list of phosphopeptide and control
457 peptides, including the Mono-isotopic precursor (m/z) and charge state (z), was generated by
458 software Skyline based on previous MS data, as shown in Table S3 (MacLean et al., 2010). The
459 peptide samples were scanned by Orbitrap Fusion Lumos mass spectrometer (Thermo Fisher
460 Scientific) with a parallel reaction monitoring (PRM) method. The PRM data were analyzed by
461 MaxQuant and Skyline, the peptides peak areas were exported for the quantification analysis.

462 **Bacterial growth assay**

463 The broad host range plasmid pBAV226 was used to express *AvrPtoB* variants in *Pseudomonas*
464 *syringae*. pBAV226 harboring *AvrPtoB* or its derivatives were transformed into the *P. syringae*
465 pv. *tomato* DC3000Δ*avrPto*Δ*avrPtoB* (DC3000 -/-) strain by electroporation (Lin and Martin,
466 2005). DC3000, DC3000 -/-, and DC3000 -/- carrying plasmids expressing *AvrPtoB* variants
467 were syringe infiltrated into five-week-old *Arabidopsis* Col-0 or *snrk2.8* leaves at a
468 concentration of 2×10^5 CFU mL^{-1} (OD600 = 0.0002). Bacterial titers were determined as
469 colony forming units (CFU) per cm^2 at four days post inoculation as previously described (Liu et
470 al., 2009).

471

472 **Callose staining and quantification**

473 Four-week-old *Arabidopsis* plants were inoculated with *Pst* DC3000, DC3000 -/-, or DC3000 -/-
474 carrying plasmids expressing *AvrPtoB* variants at a concentration of 1×10^8 CFU mL^{-1} (OD600
475 = 0.1) for 16 hr. The infected leaves were fixated and destained in 95% ethanol until they were
476 cleared of chlorophyll. The cleared leaves were washed twice with 70% ethanol and three times
477 with distilled water and stained with 1% aniline blue in 150 mM K_2HPO_4 (pH 9.5) for 30 min in
478 dark at RT. Callose deposition was imaged by fluorescence microscope (Leica CMS GmbH)
479 using a DAPI filter. Image J was used for the quantification of the number of callose (Collins,
480 2007).

481 **NPR1 and FLS2 accumulation**

482 To test the ability of AvrPtoB to inhibit NPR1 and FLS2 accumulation in *Arabidopsis* Col-0 and
483 the *snrk2.8* knockout. DC3000 -/- carrying the empty vector (EV) or a plasmid expressing wild-
484 type *AvrPtoB* were syringe infiltrated into Col-0 and *snrk2.8* at a concentration of 1×10^8 CFU
485 mL^{-1} and proteins extracted after 4h (NPR1) and 8h (FLS2). The immunoblot was performed by
486 anti-NPR1 (Agrisera #AS12 1854; 1:1000) and anti-FLS2 (Agrisera #AS12 1857; 1:5000)
487 primary antibody followed by anti-rabbit-HRP (BioRad #170-5046; 1:3000) secondary antibody.
488 Bands intensities of immunoblotting and Coomassie Brilliant Blue (CBB) staining were
489 quantified by Image Lab 6.0.1 (BIO-RAD). The values were normalized first by Rubisco bands
490 and subsequently by the intensities of "0h" bands.

491 To test the ability of AvrPtoB phosphorylation mutants to inhibit NPR1 and FLS2 accumulation,
492 *AvrPtoB* phospho-null mutants (S258A and S205AS210AS258A) and *AvrPtoB* phospho-mimic
493 mutants (S258D and S205DS210DS258D) were generated by PCR-based site-directed
494 mutagenesis. Primers are listed in Table S2. *AvrPtoB* variants were fused with C-terminal 3×
495 FLAG tag in binary vector pTA7001, and *NPR1* and *FLS2* were separately fused with C-terminal
496 HA tag and GFP tag in binary vector pEarleyGate 103 and pGWB14 (Earley et al., 2006;
497 NAKAGAWA et al., 2007). The immunoblot was performed by anti-HA HRP (Roche
498 #12013819001; 1:2,000), anti-FLAG (Sigma #A8592; 1:3000), and anti-GFP HRP (Miltenyi
499 Biotec #130-091-833; 1:3,000). Bands intensities of immunoblotting and Coomassie Brilliant
500 Blue (CBB) staining were quantified by Image Lab 6.0.1 (BIO-RAD). The values were
501 normalized first by Rubisco bands and subsequently by the intensities of "EV" bands.

502 **Plant protein extraction and immunoblotting**

503 Plant tissues were ground in liquid nitrogen and homogenized in Protein Extraction Buffer
504 [(PEB: 50 mM Tris-HCl, pH 7.5, 1 mM EDTA, pH 8.0, 150 mM NaCl, 0.1% Triton X-100,
505 0.5% IGEPAL, 5% glycerol, 1 mM PMSF, 3 mM DTT, 1 × CPI (Thermo Fisher Scientific), 1×
506 PPI (Thermo Fisher Scientific), 50 mM MG132 (Sigma-Aldrich)] (Chen et al., 2017). The
507 homogenate was cleared by centrifuging at 14,000 rpm for 15 min at 4 °C, and boiled with 5 ×
508 SDS buffer (250 mM Tris-HCl pH 6.8, 6% SDS, 0.5 M DTT, 30% glycerol, 0.08% bromophenol
509 blue) for 10 min.

510 **Statistical analyses**

511 Statistical analyses were performed by Prism 7 software (GraphPad). The data are presented as
512 mean ± SD or ± SEM as indicated in figure legends. For quantification of phosphorylated
513 peptides and quantification of NPR1 or FLS2 band intensity, n represents the number of
514 experimental replicates. For bacterial growth curve assay and callose deposition, n represents the
515 number of individual plants. Student's t test was used to compare means for two groups. One-
516 way ANOVA with Turkey's multiple-comparison test was performed to compare means from
517 several groups against a control group mean. Two-way ANOVA with Turkey's multiple-
518 comparison test was performed to compare means between groups. Statistical analyses, p-values,
519 and the exact value of n are described in detail in the figures and figure legends.

520

521 **Funding**

522 This work was supported by grants from United States Department of Agriculture: USDA-NIFA
523 2015-67013-23082 and National Institutes of Health R01: R01GM092772 awarded to G.C.

524

525 **Author Contributions**

526 G.C. conceived the study, L.L. and G.C. designed experiments, and L.L. performed most
527 experiments. D.M.S. analyzed the AvrPtoB homologs. L.L. and G.C. wrote the manuscript. All
528 authors approved of the final manuscript.

Acknowledgements

The authors thank Sheng Luan (University of California, Berkeley) for providing clones of different *SnRK* members and Michelle Salemi (University of California, Davis) for assistance in mass spectrometry analyses.

535 **References:**

536 **Abramovitch, R. B., Janjusevic, R., Stebbins, C. E., and Martin, G. B.** (2006). Type III
537 effector AvrPtoB requires intrinsic E3 ubiquitin ligase activity to suppress plant cell death and
538 immunity. *Proc National Acad Sci* **103**:2851–2856.

539 **Austin, R. S., Hiu, S., Waese, J., Ierullo, M., Pasha, A., Wang, T. T., Fan, J., Foong, C.,**
540 **Breit, R., Desveaux, D., et al.** (2016). New BAR tools for mining expression data and
541 exploring Cis -elements in Arabidopsis thaliana. *Plant J* **88**:490–504.

542 **Avila, J., Gregory, O. G., Su, D., Deeter, T. A., Chen, S., Silva-Sanchez, C., Xu, S., Martin,**
543 **G. B., and Devarenne, T. P.** (2012). The β-subunit of the SnRK1 complex is phosphorylated
544 by the plant cell death suppressor Adi3. *Plant Physiol* **159**:1277–90.

545 **Bai, X., Correa, V. R., Toruño, T. Y., Ammar, E.-D., Kamoun, S., and Hogenhout, S. A.**
546 (2009). AY-WB Phytoplasma Secretes a Protein That Targets Plant Cell Nuclei. *Mol Plant*
547 *Microbe In* **22**:18–30.

548 **Bhattacharjee, S., Noor, J. J., Gohain, B., Gulabani, H., Dnyaneshwar, I. K., and Singla, A.**
549 (2015). Post-translational modifications in regulation of pathogen surveillance and signaling
550 in plants: The inside- (and perturbations from) outside story. *Iubmb Life* **67**:524–532.

551 **Bigeard, J., Colcombet, J., and Hirt, H.** (2015). Signaling Mechanisms in Pattern-Triggered
552 Immunity (PTI). *Mol Plant* **8**:521–539.

553 **Boudsocq, M., Willmann, M. R., McCormack, M., Lee, H., Shan, L., He, P., Bush, J.,**
554 **Cheng, S.-H., and Sheen, J.** (2010). Differential innate immune signalling via Ca(2+) sensor
555 protein kinases. *Nature* **464**:418–22.

556 **Boutrot, F., and Zipfel, C.** (2017). Function, Discovery, and Exploitation of Plant Pattern
557 Recognition Receptors for Broad-Spectrum Disease Resistance. *Annu Rev Phytopathol*
558 **55**:257–286.

559 **Chen, H., Chen, J., Li, M., Chang, M., Xu, K., Shang, Z., Zhao, Y., Palmer, I., Zhang, Y.,**
560 **McGill, J., et al.** (2017). A Bacterial Type III Effector Targets the Master Regulator of
561 Salicylic Acid Signaling, NPR1, to Subvert Plant Immunity. *Cell Host Microbe* **22**:777-
562 788.e7.

563 **Chen, J., Mohan, R., Zhang, Y., Li, M., Chen, H., Palmer, I. A., Chang, M., Qi, G., Spoel, S.**
564 **H., Mengiste, T., et al.** (2019). NPR1 Promotes Its Own and Target Gene Expression in Plant
565 Defense by Recruiting CDK8. *Plant Physiol* **181**:289–304.

566 **Chinchilla, D., Zipfel, C., Robatzek, S., Kemmerling, B., Nürnberger, T., Jones, J. D. G.,**
567 **Felix, G., and Boller, T.** (2007). A flagellin-induced complex of the receptor FLS2 and
568 BAK1 initiates plant defence. *Nature* **448**:497–500.

569 **Coaker, G., Falick, A., and Staskawicz, B.** (2005). Activation of a Phytopathogenic Bacterial
570 Effector Protein by a Eukaryotic Cyclophilin. *Science* **308**:548–550.

571 **Coello, P., Hey, S. J., and Halford, N. G.** (2011). The sucrose non-fermenting-1-related
572 (SnRK) family of protein kinases: potential for manipulation to improve stress tolerance and
573 increase yield. *J Exp Bot* **62**:883–893.

574 **Collins, T. J.** (2007). ImageJ for microscopy. *Biotechniques* **43**:S25–S30.

575 **Crooks, G. E., Hon, G., Chandonia, J.-M., and Brenner, S. E.** (2004). WebLogo: A Sequence
576 Logo Generator. *Genome Res* **14**:1188–1190.

577 **Desveaux, D., Singer, A. U., Wu, A.-J., McNulty, B. C., Musselwhite, L., Nimchuk, Z.,**
578 **Sondek, J., and Dangl, J. L.** (2007). Type III Effector Activation via Nucleotide Binding,
579 Phosphorylation, and Host Target Interaction. *Plos Pathog* **3**:e48.

580 **Dubrow, Z., Sunitha, S., Kim, J.-G., Aakre, C. D., Girija, A. M., Sobol, G., Teper, D., Chen,**
581 **Y. C., Ozbaki-Yagan, N., Vance, H., et al.** (2018). Tomato 14-3-3 Proteins Are Required for
582 Xv3 Disease Resistance and Interact with a Subset of Xanthomonas euvesicatoria Effectors.
583 *Mol Plant-microbe Interactions Mpmi* **31**:1301–1311.

584 **Earley, K. W., Haag, J. R., Pontes, O., Opper, K., Juehne, T., Song, K., and Pikaard, C. S.**
585 (2006). Gateway-compatible vectors for plant functional genomics and proteomics. *Plant J*
586 **45**:616–629.

587 **Fujii, H., Verslues, P. E., and Zhu, J.-K.** (2011). Arabidopsis decuple mutant reveals the
588 importance of SnRK2 kinases in osmotic stress responses in vivo. *Proc National Acad Sci*
589 **108**:1717–1722.

590 **Gao, X., Chen, X., Lin, W., Chen, S., Lu, D., Niu, Y., Li, L., Cheng, C., McCormack, M.,**
591 **Sheen, J., et al.** (2013). Bifurcation of Arabidopsis NLR Immune Signaling via Ca2+-
592 Dependent Protein Kinases. *Plos Pathog* **9**:e1003127.

593 **Gimenez-Ibanez, S., Hann, D. R., Ntoukakis, V., Petutschnig, E., Lipka, V., and Rathjen, J.**
594 **P.** (2009). AvrPtoB targets the LysM receptor kinase CERK1 to promote bacterial virulence
595 on plants. *Curr Biology Cb* **19**:423–9.

596 **Gimenez-Ibanez, S., Boter, M., Fernández-Barbero, G., Chini, A., Rathjen, J. P., and**
597 **Solano, R.** (2014). The Bacterial Effector HopX1 Targets JAZ Transcriptional Repressors to
598 Activate Jasmonate Signaling and Promote Infection in Arabidopsis. *Plos Biol* **12**:e1001792.

599 **Göhre, V., Spallek, T., Häweker, H., Mersmann, S., Mentzel, T., Boller, T., Torres, M. de,**
600 **Mansfield, J. W., and Robatzek, S.** (2008). Plant Pattern-Recognition Receptor FLS2 Is
601 Directed for Degradation by the Bacterial Ubiquitin Ligase AvrPtoB. *Curr Biol* **18**:1824–
602 1832.

603 **Gómez-Gómez, L., and Boller, T.** (2000). FLS2: An LRR Receptor–like Kinase Involved in the
604 Perception of the Bacterial Elicitor Flagellin in Arabidopsis. *Mol Cell* **5**:1003–1011.

605 **Gu, Y., and Innes, R. W.** (2011). The KEEP ON GOING protein of Arabidopsis recruits the
606 ENHANCED DISEASE RESISTANCE1 protein to trans-Golgi network/early endosome
607 vesicles. *Plant Physiol* **155**:1827–38.

608 **Gu, Y., Zavaliev, R., and Dong, X.** (2017). Membrane Trafficking in Plant Immunity. *Mol*
609 *Plant* **10**:1026–1034.

610 **Halford, N. G., and Hey, S. J.** (2009). Snf1-related protein kinases (SnRKs) act within an
611 intricate network that links metabolic and stress signalling in plants. *Biochem J* **419**:247–59.

612 **Hardie, D. G., Ross, F. A., and Hawley, S. A.** (2012). AMPK: a nutrient and energy sensor that
613 maintains energy homeostasis. *Nat Rev Mol Cell Bio* **13**:251–262.

614 **Hayward, A. P., Tsao, J., and Dinesh-Kumar, S. P.** (2009). Autophagy and plant innate
615 immunity: Defense through degradation. *Semin Cell Dev Biol* **20**:1041–1047.

616 **Hewezi, T., Juvale, P. S., Piya, S., Maier, T. R., Rambani, A., Rice, J. H., Mitchum, M. G.,**
617 **Davis, E. L., Hussey, R. S., and Baum, T. J.** (2015). The Cyst Nematode Effector Protein
618 10A07 Targets and Recruits Host Posttranslational Machinery to Mediate Its Nuclear
619 Trafficking and to Promote Parasitism in Arabidopsis. *Plant Cell* **27**:891–907.

620 **Higashi, H., Nakaya, A., Tsutsumi, R., Yokoyama, K., Fujii, Y., Ishikawa, S., Higuchi, M.,**
621 **Takahashi, A., Kurashima, Y., Teishikata, Y., et al.** (2004). Helicobacter pylori CagA
622 Induces Ras-independent Morphogenetic Response through SHP-2 Recruitment and
623 Activation. *J Biol Chem* **279**:17205–17216.

624 **Hulsmans, S., Rodriguez, M., Coninck, B. D., and Rolland, F.** (2016). The SnRK1 Energy
625 Sensor in Plant Biotic Interactions. *Trends Plant Sci* **21**:648–61.

626 **Kim, Y. J., Lin, N.-C., and Martin, G. B.** (2002). Two Distinct Pseudomonas Effector Proteins
627 Interact with the Pto Kinase and Activate Plant Immunity. *Cell* **109**:589–598.

628 **Kim, D. S., Choi, H. W., and Hwang, B. K.** (2014). Pepper mildew resistance locus O interacts
629 with pepper calmodulin and suppresses Xanthomonas AvrBsT-triggered cell death and
630 defense responses. *Planta* **240**:827–839.

631 **Klimecka, M., and Muszyńska, G.** (2007). Structure and functions of plant calcium-dependent
632 protein kinases. *Acta Biochim Pol* **54**:219–233.

633 **Kumar, S., Stecher, G., Li, M., Knyaz, C., and Tamura, K.** (2018). MEGA X: Molecular
634 Evolutionary Genetics Analysis across Computing Platforms. *Mol Biol Evol* **35**:1547–1549.

635 **Lee, H.-J., Park, Y.-J., Seo, P. J., Kim, J.-H., Sim, H.-J., Kim, S.-G., and Park, C.-M.**
636 (2015). Systemic Immunity Requires SnRK2.8-Mediated Nuclear Import of NPR1 in
637 Arabidopsis. *Plant Cell* **27**:3425–3438.

638 **Li, W., Yadeta, K. A., Elmore, J. M., and Coaker, G.** (2013). The Pseudomonas syringae
639 Effector HopQ1 Promotes Bacterial Virulence and Interacts with Tomato 14-3-3 Proteins in a
640 Phosphorylation-Dependent Manner. *Plant Physiol* **161**:2062–2074.

641 **Lin, N.-C., and Martin, G. B.** (2005). An avrPto/avrPtoB Mutant of Pseudomonas syringae pv.
642 tomato DC3000 Does Not Elicit Pto-Mediated Resistance and Is Less Virulent on Tomato.
643 *Mol Plant Microbe In* **18**:43–51.

644 **Liu, J., Elmore, J. M., Fuglsang, A. T., Palmgren, M. G., Staskawicz, B. J., and Coaker, G.**
645 (2009). RIN4 Functions with Plasma Membrane H+-ATPases to Regulate Stomatal Apertures
646 during Pathogen Attack. *Plos Biol* **7**:e1000139.

647 **Lolle, S., Stevens, D., and Coaker, G.** (2020). Plant NLR-triggered immunity: from receptor
648 activation to downstream signaling. *Curr Opin Immunol* **62**:99–105.

649 **Lu, D., Lin, W., Gao, X., Wu, S., Cheng, C., Avila, J., Heese, A., Devarenne, T. P., He, P.,**
650 **and Shan, L.** (2011). Direct Ubiquitination of Pattern Recognition Receptor FLS2 Attenuates
651 Plant Innate Immunity. *Science* **332**:1439–1442.

652 **Macho, A. P., Schwessinger, B., Ntoukakis, V., Brutus, A., Segonzac, C., Roy, S., Kadota,**
653 **Y., Oh, M.-H., Sklenar, J., Derbyshire, P., et al.** (2014). A Bacterial Tyrosine Phosphatase
654 Inhibits Plant Pattern Recognition Receptor Activation. *Science* **343**:1509–1512.

655 **MacLean, B., Tomazela, D. M., Shulman, N., Chambers, M., Finney, G. L., Frewen, B.,**
656 **Kern, R., Tabb, D. L., Liebler, D. C., and MacCoss, M. J.** (2010). Skyline: an open source
657 document editor for creating and analyzing targeted proteomics experiments. *Bioinform Oxf*
658 *Engl* **26**:966–8.

659 **Martin, G.** (2011). Suppression and Activation of the Plant Immune System by Pseudomonas
660 syringae Effectors AvrPto and AvrPtoB. *Effectors in Plant-Microbe Interactions* Advance
661 Access published 2011, doi:ch6.

662 **Mergner, J., Frejno, M., List, M., Papacek, M., Chen, X., Chaudhary, A., Samaras, P.,**
663 **Richter, S., Shikata, H., Messerer, M., et al.** (2020). Mass-spectrometry-based draft of the
664 Arabidopsis proteome. *Nature* Advance Access published 2020, doi:10.1038/s41586-020-
665 2094-2.

666 **Minkoff, B. B., Burch, H. L., and Sussman, M. R.** (2013). Methods in Molecular Biology.
667 *Methods Mol Biology Clifton N J* **1062**:353–379.

668 **NAKAGAWA, T., SUZUKI, T., MURATA, S., NAKAMURA, S., HINO, T., MAEO, K.,**
669 **TABATA, R., KAWAI, T., TANAKA, K., NIWA, Y., et al.** (2007). Improved Gateway
670 Binary Vectors: High-Performance Vectors for Creation of Fusion Constructs in Transgenic
671 Analysis of Plants. *Biosci Biotechnology Biochem* **71**:2095–2100.

672 **Nakano, M., and Mukaihara, T.** (2019). Comprehensive Identification of PTI Suppressors in
673 Type III Effector Repertoire Reveals that Ralstonia solanacearum Activates Jasmonate
674 Signaling at Two Different Steps. *Int J Mol Sci* **20**:5992.

675 **Nougayrede, J.-P., Fernandes, P. J., and Donnenberg, M. S.** (2003). Adhesion of
676 enteropathogenic Escherichia coli to host cells. *Cell Microbiol* **5**:359–372.

677 **Peng, Y., Wersch, R. van, and Zhang, Y.** (2018). Convergent and Divergent Signaling in
678 PAMP-Triggered Immunity and Effector-Triggered Immunity. *Mol Plant-microbe*
679 *Interactions Mpmi* **31**:403–409.

680 **Rosebrock, T. R., Zeng, L., Brady, J. J., Abramovitch, R. B., Xiao, F., and Martin, G. B.**
681 (2007). A bacterial E3 ubiquitin ligase targets a host protein kinase to disrupt plant immunity.
682 *Nature* **448**:370–374.

683 **Schornack, S., Moscou, M. J., Ward, E. R., and Horvath, D. M.** (2013). Engineering plant
684 disease resistance based on TAL effectors. *Annu Rev Phytopathol* **51**:383–406.

685 **Shan, L., He, P., Li, J., Heese, A., Peck, S. C., Nürnberger, T., Martin, G. B., and Sheen, J.**
686 (2008). Bacterial Effectors Target the Common Signaling Partner BAK1 to Disrupt Multiple
687 MAMP Receptor-Signaling Complexes and Impede Plant Immunity. *Cell Host Microbe* **4**:17–
688 27.

689 **Shen, Q., Liu, Z., Song, F., Xie, Q., Hanley-Bowdoin, L., and Zhou, X.** (2011). Tomato
690 SlSnRK1 protein interacts with and phosphorylates βC1, a pathogenesis protein encoded by a
691 geminivirus β-satellite. *Plant Physiol* **157**:1394–406.

692 **Shin, R., Alvarez, S., Burch, A. Y., Jez, J. M., and Schachtman, D. P.** (2007).
693 Phosphoproteomic identification of targets of the Arabidopsis sucrose nonfermenting-like
694 kinase SnRK2.8 reveals a connection to metabolic processes. *Proc National Acad Sci*
695 **104**:6460–6465.

696 **Streubel, J., Pesce, C., Hutin, M., Koebnik, R., Boch, J., and Szurek, B.** (2013). Five
697 phylogenetically close rice SWEET genes confer TAL effector-mediated susceptibility to
698 Xanthomonas oryzae pv. oryzae. *New Phytol* **200**:808–819.

699 **Szczesny, R., Büttner, D., Escolar, L., Schulze, S., Seiferth, A., and Bonas, U.** (2010).
700 Suppression of the AvrBs1-specific hypersensitive response by the YopJ effector homolog
701 AvrBsT from Xanthomonas depends on a SNF1-related kinase. *New Phytol* **187**:1058–1074.

702 **Szurek, B., Marois, E., Bonas, U., and Ackerveken, G. V. den** (2001). Eukaryotic features of
703 the Xanthomonas type III effector AvrBs3: protein domains involved in transcriptional
704 activation and the interaction with nuclear import receptors from pepper. *Plant J* **26**:523–534.

705 **Tahir, J., Rashid, M., and Afzal, A. J.** (2019). Post-translational modifications in effectors and
706 plant proteins involved in host–pathogen conflicts. *Plant Pathol* **68**:628–644.

707 **Tarrant, M. K., and Cole, P. A.** (2009). The Chemical Biology of Protein Phosphorylation.
708 *Annu Rev Biochem* **78**:797–825.

709 **Taylor, K. W., Kim, J.-G., Su, X. B., Aakre, C. D., Roden, J. A., Adams, C. M., and**
710 **Mudgett, M. B.** (2012). Tomato TFT1 Is Required for PAMP-Triggered Immunity and
711 Mutations that Prevent T3S Effector XopN from Binding to TFT1 Attenuate Xanthomonas
712 Virulence. *Plos Pathog* **8**:e1002768.

713 **Torres, M. de, Mansfield, J. W., Grabov, N., Brown, I. R., Ammouneh, H., Tsiamis, G.,**
714 **Forsyth, A., Robatzek, S., Grant, M., and Boch, J.** (2006). Pseudomonas syringae effector
715 AvrPtoB suppresses basal defence in Arabidopsis. *Plant J* **47**:368–382.

716 **Toruño, T. Y., Stergiopoulos, I., and Coaker, G.** (2015). Plant Pathogen Effectors: Cellular
717 Probes Interfering with Plant Defenses in Spatial and Temporal Manners. *Annu Rev*
718 *Phytopathol* **54**:1–23.

719 **Tran, T. T., Pérez-Quintero, A. L., Wonni, I., Carpenter, S. C. D., Yu, Y., Wang, L., Leach,**
720 **J. E., Verdier, V., Cunnac, S., Bogdanove, A. J., et al.** (2018). Functional analysis of
721 African Xanthomonas oryzae pv. oryzae TALomes reveals a new susceptibility gene in
722 bacterial leaf blight of rice. *Plos Pathog* **14**:e1007092.

723 **Tyanova, S., Temu, T., and Cox, J.** (2016). The MaxQuant computational platform for mass
724 spectrometry-based shotgun proteomics. *Nat Protoc* **11**:2301–2319.

725 **Umezawa, T., Yoshida, R., Maruyama, K., Yamaguchi-Shinozaki, K., and Shinozaki, K.**
726 (2004). SRK2C, a SNF1-related protein kinase 2, improves drought tolerance by controlling
727 stress-responsive gene expression in Arabidopsis thaliana. *P Natl Acad Sci Usa* **101**:17306–
728 17311.

729 **Vlad, F., Turk, B. E., Peynot, P., Leung, J., and Merlot, S.** (2008). A versatile strategy to
730 define the phosphorylation preferences of plant protein kinases and screen for putative
731 substrates. *Plant J* **55**:104–117.

732 **Wang, W., Liu, N., Gao, C., Rui, L., and Tang, D.** (2019). The Pseudomonas Syringae
733 Effector AvrPtoB Associates With and Ubiquitinates Arabidopsis Exocyst Subunit
734 EXO70B1. *Front Plant Sci* **10**:1027.

735 **Wirthmueller, L., Roth, C., Fabro, G., Caillaud, M.-C., Rallapalli, G., Asai, S., Sklenar, J.,**
736 **Jones, A. M. E., Wiermer, M., Jones, J. D. G., et al.** (2014). Probing formation of
737 cargo/importin-α transport complexes in plant cells using a pathogen effector. *Plant J* **81**:40–
738 52.

739 **Withers, J., and Dong, X.** (2016). Posttranslational Modifications of NPR1: A Single Protein
740 Playing Multiple Roles in Plant Immunity and Physiology. *Plos Pathog* **12**:e1005707.

741 **Withers, J., and Dong, X.** (2017). Post-translational regulation of plant immunity. *Curr Opin*
742 *Plant Biol* **38**:124–132.

743 **Xiang, T., Zong, N., Zou, Y., Wu, Y., Zhang, J., Xing, W., Li, Y., Tang, X., Zhu, L., Chai,**
744 **J., et al.** (2008). Pseudomonas syringae Effector AvrPto Blocks Innate Immunity by
745 Targeting Receptor Kinases. *Curr Biol* **18**:74–80.

746 **Xiao, F., He, P., Abramovitch, R. B., Dawson, J. E., Nicholson, L. K., Sheen, J., and Martin,**
747 **G. B.** (2007a). The N-terminal region of Pseudomonas type III effector AvrPtoB elicits Pto-
748 dependent immunity and has two distinct virulence determinants. *Plant J* **52**:595–614.

749 **Xiao, F., Giavalisco, P., and Martin, G. B.** (2007b). Pseudomonas syringae Type III Effector
750 AvrPtoB Is Phosphorylated in Plant Cells on Serine 258, Promoting Its Virulence Activity. *J*
751 *Biol Chem* **282**:30737–30744.

752 **Xing, T., Ouellet, T., and Miki, B. L.** (2002). Towards genomic and proteomic studies of
753 protein phosphorylation in plant–pathogen interactions. *Trends Plant Sci* **7**:224–230.

754 **Yoo, S.-D., Cho, Y.-H., and Sheen, J.** (2007). Arabidopsis mesophyll protoplasts: a versatile
755 cell system for transient gene expression analysis. *Nat Protoc* **2**:1565–1572.

756 **Zhang, T., Lei, J., Yang, H., Xu, K., Wang, R., and Zhang, Z.** (2011). An improved method
757 for whole protein extraction from yeast Saccharomyces cerevisiae. *Yeast Chichester Engl*
758 **28**:795–8.

759 **Zhou, B., Mural, R. V., Chen, X., Oates, M. E., Connor, R. A., Martin, G. B., Gough, J.,**
760 **and Zeng, L.** (2016). A Subset of Ubiquitin-Conjugating Enzymes Is Essential for Plant
761 Immunity. *Plant Physiol* **173**:1371–1390.

762

763

764 **Figure legends**

765 **Figure 1. The *Pseudomonas syringae* effector AvrPtoB interacts with the plant kinase**
766 **SnRK2.8.**

767 (A) Phylogeny of the *Arabidopsis* SnRK family and transcript expression of *SnRK* members after
768 immune activation and pathogen infection. Phylogeny was determined by maximum likelihood
769 method (1000 bootstrap replicates). The heat map shows fold change in leaf transcript expression
770 one-hour post-treatment with SA, one hour post-treatment with flg22, and six hours post-
771 infiltration with *Pseudomonas syringae* pv. *tomato* strain *hrcC*. The bar graph represents the
772 *SnRK* expression in leaf tissue. Data were obtained from BAR Expression Angler. Blue dots
773 represent the *SnRK* members that were cloned for yeast-two hybrid. hrcC = *P. syringae* pv.
774 *tomato* DC3000 *hrcC* mutant defective in Type III secretion system.

775 (B, C) Yeast two-hybrid assay of AvrPtoB and SnRK-CDPKs. AvrPtoB was co-expressed with
776 Pto, SnRK3.1, SnRK1.1, SnRK2.6, SnRK2.8, as well as a C-terminal deletion of CPK4
777 (CPK4△C) and CPK5 (CPK5△C) in yeast. Empty vector (EV) and AD-mCherry were included
778 as negative controls. Colony growth on SD -Leu/-Trp media confirms the presence of AD and
779 BD vectors. Growth on SD -Leu/-Trp/-His media indicates protein-protein interaction. AD =
780 activation domain vector, BD = binding domain vector.

781 (D, E) Co-immunoprecipitation (Co-IP) of AvrPtoB-GFP with SnRK/CPK△C kinase dead
782 (KD)-HA variants in *N. benthamiana*. *AvrPtoB-GFP* under control of a dexamethasone (Dex)-
783 inducible promoter was co-expressed with *35S::SnRKs-KD-HA* and *35S::CPKs△C-KD-HA* in *N.*
784 *benthamiana* using Agrobacterium-mediated transient expression. Expression of *AvrPtoB-GFP*
785 was induced by 15 μM DEX for three hours at 24 hours post-infiltration. Protein extracts were
786 subjected to anti-GFP immunoprecipitation (IP). The IP and input proteins were immunoblotted
787 with anti-HA and anti-GFP antibodies.

788

789 **Figure 2. AvrPtoB is phosphorylated by SnRK2.8.**

790 (A) *In vitro* kinase activity assay of AvrPtoB and SnRK2.8. Recombinant GST-AvrPtoB and
791 GST-SnRK2.8 proteins were purified from *E. coli* and incubated with ATP in kinase buffer for

792 30 min. Phosphorylation was detected by anti-pSer/Thr (anti-pS/T) immunoblot. Coomassie
793 Brilliant Blue (CBB) staining shows protein loading.

794 (B) AvrPtoB phosphorylation sites identified *in vivo* by LC-MS/MS. AvrPtoB-GFP was
795 transiently expressed in *Arabidopsis* Col-0 protoplasts and total proteins were subjected to anti-
796 GFP IP followed by trypsin digestion. Phosphorylated peptides were detected by LC-MS/MS.
797 The observed y and b ions are numbered.

798 (C) Diagram of phosphorylation sites and host protein interaction domains in AvrPtoB. PID
799 (green) indicates the Pto interaction domain, NID (blue) indicates the NPR1 interaction domain,
800 BID (black slash) indicates the BAK1 interaction domain and FID (yellow) indicates the Fen
801 interaction domain. Numbers correspond to amino acid (aa) residues.

802 (D) Quantification of S258, S210 and S205 phosphorylation. AvrPtoB-GFP was expressed in
803 Col-0 and *snrk2.8* protoplasts and total proteins were subjected to anti-GFP IP followed by
804 tryptic digestion. Phosphorylated peptides were detected by LC-MS/MS with the parallel
805 reaction monitoring method. Peptide phosphorylation ratios (phosphorylated/non-
806 phosphorylated) were determined using Skyline software. Data are means ± SE of three
807 biological replicates (separate transfections). Asterisks indicate significant differences (Student's
808 t-test, $^{**}p<0.01$).

809

810 **Figure 3. SnRK2.8 is required for AvrPtoB virulence.**

811 (A) Disease symptoms of *Arabidopsis* Col-0 and the *snrk2.8* knockout after infection with *P.*
812 *syringae* pv. *tomato* DC3000 (DC3000) variants. DC3000 and DC3000Δ*avrPto*Δ*avrPtoB* (-/-)
813 carrying empty vector (EV) or expressing *AvrPtoB* on a plasmid were syringe infiltrated into
814 *Arabidopsis* Col-0 and *snrk2.8* at a concentration of 2×10^5 CFU mL^{-1}. Disease symptoms were
815 observed 4 days post-inoculation (dpi).

816 (B) Bacterial populations in Col-0 and *snrk2.8* leaves 4 dpi. Bacterial inoculations were
817 performed as described in (A). LOG CFU/cm^2 = log colony forming units per cm^2 of leaf tissue.
818 Data are means ± SD ($n \geq 9$ plants for day 0, $n \geq 18$ plants for day 4). Different letters indicate
819 significant differences (two-way ANOVA, Tukey's test, $p < 0.05$).

820 (C) Callose deposition in *Arabidopsis* Col-0 and *snrk2.8* after inoculation with DC3000, -/- EV,
821 and -/-*AvrPtoB*. Leaves were inoculated with *P. syringae* at a concentration of 1×10^8 CFU mL^{-1}
822 and harvested 16h later. Leaves were stained by 1% aniline blue and imaged by fluorescence
823 microscopy. Scale bar, 100 µm.

824 (D) Quantification of callose deposits. Data from three independent experiments were used for
825 statistical analysis. Data are means ± SD (n = 24 images from 24 leaves). Different letters
826 indicate significant differences (two-way ANOVA, Tukey's test, $p < 0.05$).

827

828 **Figure 4. Phosphorylated AvrPtoB serine residues are required for virulence.**

829 (A) Disease symptoms of *Arabidopsis* Col-0 after inoculation with *P. syringae* pv. *tomato*
830 DC3000Δ*avrPto*Δ*avrPtoB* (-/-) variants. DC3000 -/- carrying empty vector (EV) or plasmids
831 expressing wild-type *AvrPtoB*, $AvrPtoB_{S258A}$, or $AvrPtoB_{S205AS210AS258A}$ (*SSSAAA*) were syringe
832 infiltrated into *Arabidopsis* Col-0 at a concentration of 2×10^5 CFU mL^{-1}. Disease symptoms
833 were observed 4 days post-inoculation (dpi).

834 (B) Bacterial populations in Col-0 leaves 4 dpi. Bacterial inoculations were performed as
835 described in (A). LOG CFU/cm^2 = log colony-forming units per cm^2 of leaf tissue. Data are
836 means ± SD (n = 4 plants for day 0, n = 8 plants for day 4). Different letters indicate significant
837 differences (two-way ANOVA, Tukey's test, $p < 0.05$).

838 (C) Callose deposition in *Arabidopsis* Col-0 after inoculation with -/- carrying EV, *AvrPtoB*,
839 *S258A*, and *SSSAAA*. Leaves were inoculated with *P. syringae* at a concentration of 1×10^8 CFU
840 mL^{-1} and harvested 16h later. Leaves were stained by 1% aniline blue and imaged by
841 fluorescence microscopy. Scale bar, 100 µm.

842 (D) Quantification of callose deposits. Data are means ± SD (n = 8 images from 8 leaves for -/-
843 EV, n =18 images from 18 leaves for rest variants). Different letters indicate significant
844 differences (one-way ANOVA, Tukey's test, $p < 0.05$).

845

846 **Figure 5. AvrPtoB mediated degradation of NPR1 requires the plant kinase SnRK2.8.**

847 (A) NPR1 accumulation in *Arabidopsis* Col-0 and the *snrk2.8* knockout after inoculation with *P.*
848 *syringae* pv. *tomato* DC3000Δ*avrPto*Δ*avrPtoB* (-/-) variants. DC3000 -/- carrying the empty
849 vector (EV) or a plasmid expressing wild-type *AvrPtoB* were syringe infiltrated into Col-0 and
850 *snrk2.8* at a concentration of 1×10^8 CFU mL^{-1} and proteins extracted after four hours. Protein
851 extracts were subjected to anti-NPR1 immunoblotting. Coomassie Brilliant Blue (CBB) staining
852 shows equal protein loading.

853 (B) Quantification of NPR1 band intensity in (A). NPR1 bands intensities were quantified by
854 Image Lab 6.0.1 (BIO-RAD). The values were normalized first by Rubisco bands and
855 subsequently by the intensities of "0h" bands. Data are means ± SD (n = 14 leaves). Different
856 letters indicate significant differences (one-way ANOVA, Tukey's test, $p < 0.05$).

857 (C) NPR1 accumulation in the presence of AvrPtoB phosphorylation mutants in *N. benthamiana*
858 after Agrobacterium-mediated transient expression. *35S::NPR1-HA* was co-expressed with
859 FLAG-tagged Dex-inducible *AvrPtoB*, $AvrPtoB_{S258A}$, $AvrPtoB_{S205AS210AS258A}$ (*SSSAAA*),
860 $AvrPtoB_{S258D}$ or $AvrPtoB_{S205DS210DS258D}$ (*SSSDDD*). The Dex inducible EV was used as a control.
861 The expression of AvrPtoB-FLAG phosphorylation variants was induced by 15 μM DEX for 5
862 hours 24h post-Agrobacterium infiltration. Protein extracts were subjected to anti-HA and anti-
863 FLAG immunoblotting. CBB staining shows protein loading.

864 (D) Quantification of NPR1-HA band intensity in (C). NPR1-HA bands intensities were
865 quantified by Image Lab 6.0.1. The values were normalized first by Rubisco bands and
866 subsequently by the intensities of "EV" treatment. Data are means ± SD (n = 6 leaves). Different
867 letters indicate significant differences (one-way ANOVA, Tukey's test, $p < 0.05$).

868

869 **Figure 6. AvrPtoB-mediated degradation of FLS2 and inhibition of FLS2 complex**
870 **formation requires the plant kinase SnrK2.8 and phosphorylated residues.**

871 (A) FLS2 accumulation in *Arabidopsis* Col-0 and the *snrk2.8* knockout after inoculation with *P.*
872 *syringae* pv. *tomato* DC3000Δ*avrPto*Δ*avrPtoB* (-/-) variants. DC3000 -/- carrying the empty
873 vector (EV) or a plasmid expressing wild-type *AvrPtoB* were syringe infiltrated into Col-0 and
874 *snrk2.8* at a concentration of 1×10^8 CFU mL^{-1} and proteins extracted after 8h. Protein extracts

875 were subjected to anti-FLS2 immunoblotting. Coomassie Brilliant Blue (CBB) staining shows
876 equal protein loading.

877 (B) Quantification of FLS2 band intensity in (A). FLS2 band intensities were quantified by
878 Image Lab 6.0.1. The values were normalized first by Rubisco bands and subsequently by the
879 intensities of "0h" bands. Data are means ± SD (n = 14 leaves). Different letters indicate
880 significant differences (one-way ANOVA, Tukey's test, $p < 0.05$).

881 (C) FLS2 accumulation in the presence of AvrPtoB phosphorylation mutants in *N. benthamiana*
882 after Agrobacterium-mediated transient expression. *35S::FLS2-GFP* was co-expressed with
883 FLAG-tagged Dex-inducible *AvrPtoB*, *AvrPtoB*$_{S258A}$, *AvrPtoB*$_{S205AS210AS258A}$ (*SSSAAA*),
884 *AvrPtoB*$_{S258D}$, or *AvrPtoB*$_{S205DS210DS258D}$ (*SSSDDD*). The Dex inducible EV was used as a control.
885 The expression of AvrPtoB-FLAG phosphorylation variants was induced by 15 μM DEX for 5
886 hours 24h post-Agrobacterium infiltration. Protein extracts were subjected to anti-GFP and anti-
887 FLAG immunoblotting. CBB staining shows protein loading.

888 (D) Quantification of FLS2-GFP band intensity in (C). FLS2-GFP bands intensities were
889 quantified by Image Lab 6.0.1. The values were normalized first by Rubisco bands and
890 subsequently by the intensities of "EV" treatment. The data from two independent experiments
891 were used for statistical analysis. Data are means ± SD (n = 6 leaves). Different letters indicate
892 significant differences (one-way ANOVA, Tukey's test, $p < 0.05$).

893 (E) Analyses of AvrPtoB-mediated inhibition of FLS2 complex formation. AvrPtoB-FLAG
894 variants, BAK1-HA, and FLS2-GFP were co-expressed in the indicated combinations in *N.*
895 *benthamiana* using Agrobacterium-mediated transient expression. The expression of AvrPtoB-
896 FLAG phosphorylation variants was induced by 15 μM DEX for 3 hours 24h post-
897 Agrobacterium infiltration. Leaves were infiltrated with 10 μM flg22 peptide 15 minutes before
898 harvesting protein extracts for GFP immunoprecipitation and western blotting. Protein inputs and
899 immunoprecipitated samples were detected by immunoblot.

900

901 **Supplemental Table and Figure Legends.**

902

903 **Supplemental Table 1. The phosphorylation sites of bacterial type III effectors identified by**
904 **mass spectrometry. Related to Figure 1.** Data were collected from the references in the table.
905 Red indicates the phosphorylated residue.

906

907 **Supplemental Table 2. Primers used in this study. Related to Materials and Methods.**

908

909 **Supplemental Table 3. Isolation list for PRM. Related to Figure 2.** Modified and unmodified
910 peptide sequences used to quantify phosphorylation by PRM are noted. CID = collision induced
911 dissociation, m/z = mass to charge, z = charge state.

912

913 **Supplemental Figure 1. Amino acid conservation surrounding known effector**
914 **phosphorylation sites. Related to Figure 1.**

915 WebLogo alignment of the effector phosphorylation sites shown in Table S1. Red arrows point
916 the phosphorylated residues. Amino acid size correlates with degree of conservation. The
917 sequence logo was created by the WebLogo 3 (Crooks et al., 2004).

918

919 **Supplemental Figure 2. Yeast-two hybrid screening of interactions between the**
920 ***Pseudomonas syringae* effector AvrPtoB and SnRK or CDPK members. Related to Figure**
921 **1.**

922 Yeast two-hybrid (Y2H) assay of AvrPtoB and SnRK-CDPKs in the Matchmaker GaL4 system.
923 AvrPtoB was expressed from the pGADT7 vector, while SnRKs and C-terminal deletions of
924 CPKs (CPKs△C) were expressed from the pGBKT7 vector in *Saccharomyces cerevisea.* The
925 pGBKT7 empty vector (EV) was included as a negative control. Blue colonies on SD -Leu/-

926 Trp/-His/X-α-gal media indicate protein-protein interactions. AD = activation domain vector
927 pGADT7, BD = binding domain vector pGBKT7.

928

929 **Supplemental Figure 3. Protein expression of *SnRKs*, *CPKs*, and *AvrPtoB* used in the Y2H**
930 **assay. Related to Figure 1.**

931 Yeast proteins were extracted and SnRK and CPK proteins were detected by anti-myc
932 immunoblot and AvrPtoB was detected by anti-HA immunoblot. Expression of the positive (Pto)
933 and negative (mCherry) controls used in Figure 1 are shown.

934

935 **Supplemental Figure 4. AvrPtoB T111 and S217 phosphorylation are not lower in the**
936 ***snrk2.8* knockout compared to wild-type Col-0. Related to Figure 2.**

937 AvrPtoB-GFP was expressed in Col-0 and *snrk2.8* protoplasts, total proteins were subjected to
938 anti-GFP IP followed by tryptic digestion. Phosphorylated peptides were detected by LC-MS/MS
939 with the parallel reaction monitoring method. The peptide phosphorylation intensity of T111 (A)
940 and the phosphorylation ratio of S217 (B) were determined using Skyline software. Data are
941 means ± SE of three biological replicates (separate transfections). Asterisks indicate significant
942 differences (Student's t-test, **$p<0.01$).

943

944 **Supplemental Figure 5. Conservation of phosphorylated residues in different AvrPtoB**
945 **homologs. Related to Figure 2.**

946 The AvrPtoB phosphorylated residues identified by mass spectrometry were analyzed for their
947 conservation across 27 AvrPtoB homologs from *P. syringae.* The translated sequence of
948 AvrPtoB was used in BLAST searches against the NCBI nr database on January 5th, 2020
949 (*Pseudomonas syringae* group, taxid: 136849; default parameters otherwise) to identify
950 homologs. Hits were filtered based on a minimum 65% sequence identity, a minimum 85%
951 query coverage and an E-value of 0. Sequences were downloaded and aligned using Genious
952 alignment (default parameters).The percentage of identity is shown by gradient white to black
953 (white means less than 60% similar, gray means 60-80% similar, dark gray means 80-100%, and

954 black means 100% similar). AvrPtoB phosphorylation sites identified *in vivo* are shown with
955 arrows.

956

957 **Supplemental Figure 6. AvrPtoB S258 is required for virulence in tomato and *Arabidopsis*.**
958 **Related to Figure 3.**

959 (A) Bacterial populations in the susceptible tomato genotype Rio Grande 76S five days post-
960 inoculation with *P. syringae* pv. *tomato* DC3000Δ*avrPto*Δ*avrPtoB* (-/-) variants. DC3000 -/-
961 carrying empty vector (EV) or plasmids expressing wild-type *AvrPtoB*, $AvrPtoB_{S258A}$, $AvrPtoB_{1-}$
962 $_{307}$, and $AvrPtoB_{1-307S258A}$ were dip inoculated on tomato at a concentration of 2×10^8 CFU mL^{-1}
963 with 0.005% Silwet. LOG CFU/cm^2 = log colony-forming units per cm^2 of leaf tissue. Data are
964 means ± SD ($n \geq 6$ plants). Different letters indicate significant differences (one-way ANOVA,
965 Tukey's test, $p < 0.05$).

966 (B) Bacterial populations in *Arabidopsis* Col-0 three days post-inoculation with DC3000 -/-
967 variants. DC3000 -/- variants as described in (A) were syringe infiltrated in Col-0 at a
968 concentration of 2×10^5 CFU mL^{-1}. Data are means ± SD (n = 4 plants for day 0, n = 6 plants for
969 day 3). Different letters indicate significant differences (two-way ANOVA, Tukey's test, $p <$
970 0.05).

971 (C) Expression of AvrPtoB and its derivatives from DC3000 -/- . Bacteria were grown in
972 minimal media at 18 °C. Anti-HA western blotting was performed to detect the expression of
973 AvrPtoB in bacterial pellets.

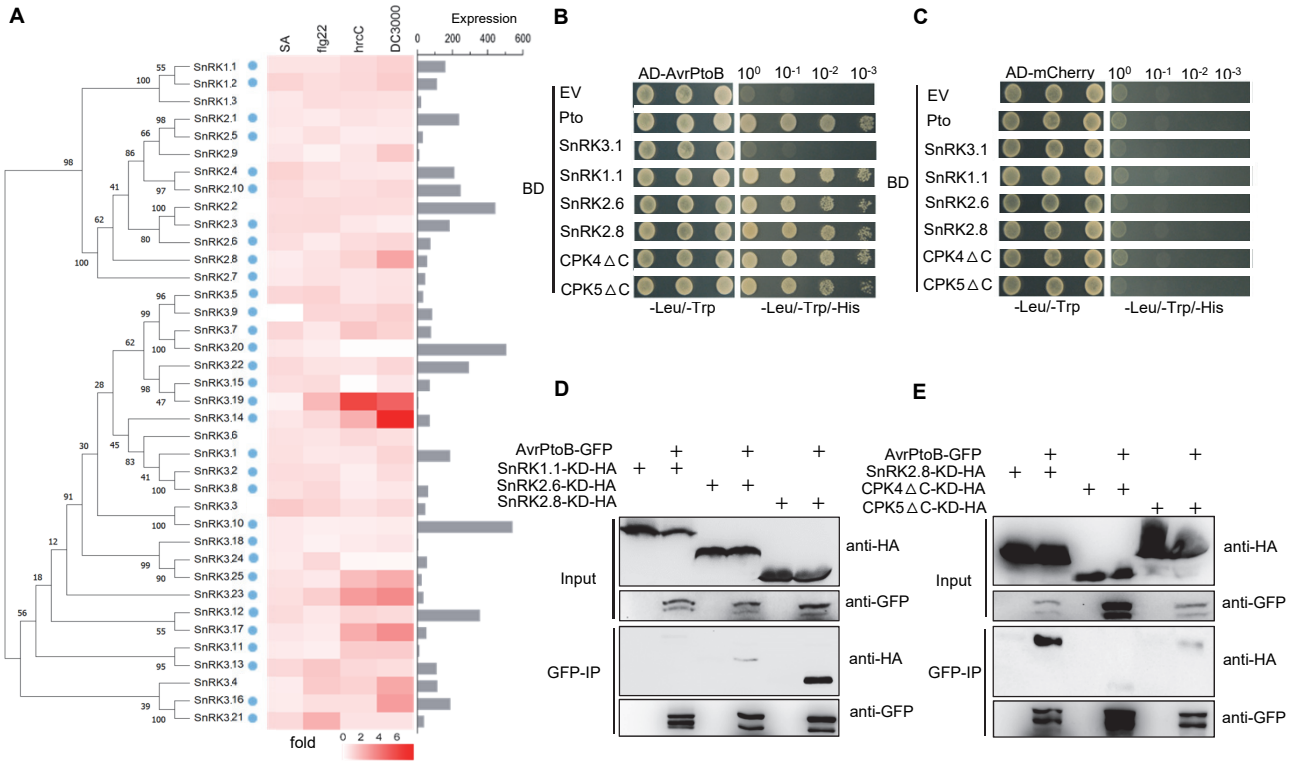

Figure 1. The *Pseudomonas syringae* effector AvrPtoB interacts with the plant kinase SnRK2.8.

(A) Phylogeny of the *Arabidopsis* SnRK family and transcript expression of *SnRK* members after immune activation and pathogen infection. The phylogeny was determined by maximum likelihood method (1000 bootstrap replicates). The heat map shows fold change in leaf transcript expression one-hour post-treatment with SA, one hour post-treatment with and flg22, and six hours post-infiltration with *Pseudomonas syringae* pv. *tomato* strain DC3000. The bar graph represents the leaf gene expression. Data was obtained from BAR Expression Angler. Blue dots represent the SnRK members that were cloned for yeast-two hybrid. hrcC = *P. syringae* pv. *tomato* DC3000 hrcC mutant defective in Type III secretion system.
(B, C) Yeast two-hybrid assay of AvrPtoB and SnRK-CDPKs. AvrPtoB was co-expressed with Pto, SnRK3.1, SnRK1.1, SnRK2.6, SnRK2.8, as well as a C terminal deletion of CPK4 (CPK4△C) and CPK5 (CPK5△C) in yeast. Empty vector (EV) and AD-mCherry were included as negative controls. Colony growth on SD -Leu/-Trp media confirms the presence of AD and BD vectors. Growth on SD -Leu/-Trp/-His media indicates protein-protein interaction. AD = activation domain vector, BD = binding domain vector.
(D, E) Co-immunoprecipitation (co-IP) of AvrPtoB-GFP with SnRK/ CPK△C kinase dead (KD)-HA variants in *N. benthamiana*. *AvrPtoB-GFP* under control of a dexamethasone (Dex)-inducible promoter was co-expressed with *35S::SnRKs-KD-HA* and *35S::CPKs△C-KD-HA* in *N. benthamiana* using Agrobacterium-mediated transient expression. Expression of *AvrPtoB-GFP* was induced by 15 µM DEX for three hours at 24 hours post-infiltration. Protein extracts were subjected to anti-GFP immunoprecipitation (IP). The IP and input proteins were immunoblotted with anti-HA and anti-GFP antibodies.

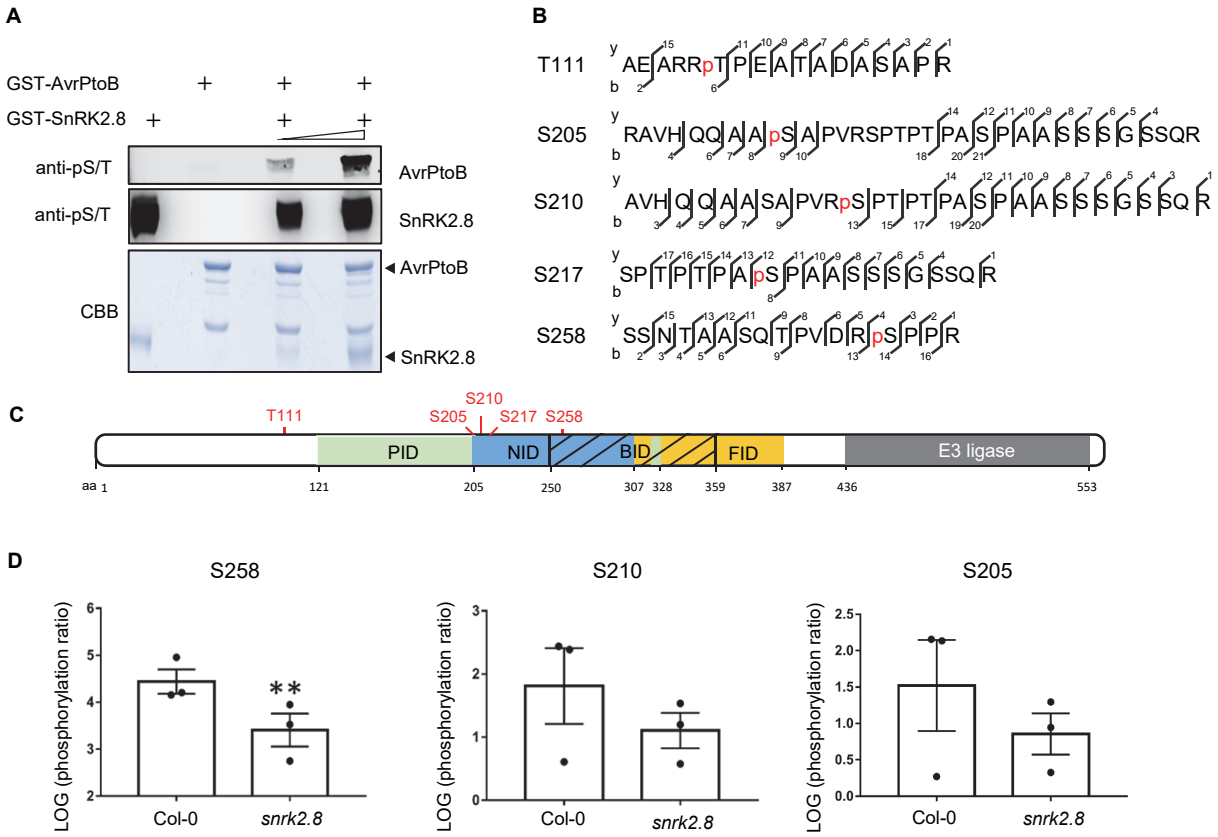

Figure 2. AvrPtoB is phosphorylated by SnRK2.8.

(A) *In vitro* kinase activity assay of AvrPtoB and SnRK2.8. Recombinant GST-AvrPtoB and GST-SnRK2.8 proteins were purified from *E. coli* and incubated with ATP in kinase buffer for 30 min. Phosphorylation was detected by anti-pSer/Thr (anti-pS/T) immunoblot, Coomassie Brilliant Blue (CBB) staining shows protein loading.
(B) AvrPtoB phosphorylation sites identified *in vivo* by LC-MS/MS. AvrPtoB-GFP was transiently expressed in *Arabidopsis* Col-0 protoplasts and total proteins were subjected to anti-GFP IP followed by trypsin digestion. Phosphorylated peptides were detected by LC-MS/MS. The observed y and b ions are numbered.
(C) Diagram of phosphorylation sites and host protein interaction domains in AvrPtoB. PID (green) indicates the Pto interaction domain, NID (blue) indicates the NPR1 interaction domain, BID (black slash) indicates the BAK1 interaction domain and FID (yellow) indicates the Fen interaction domain. Numbers correspond to amino acid (aa) residues.
(D) Quantification of S258, S210 and S205 phosphorylation. AvrPtoB-GFP was expressed in Col-0 and *snrk2.8* protoplasts and total proteins were subjected to anti-GFP IP followed by tryptic digestion. Phosphorylated peptides were detected by LC-MS/MS with the parallel reaction monitoring method. Peptide phosphorylation ratios (phosphorylated/non-phosphorylated) were determined using Skyline software. Data are means ± SE of three biological replicates (separate transfections). Asterisks indicate significant differences (Student's t-test, **$p<0.01$).

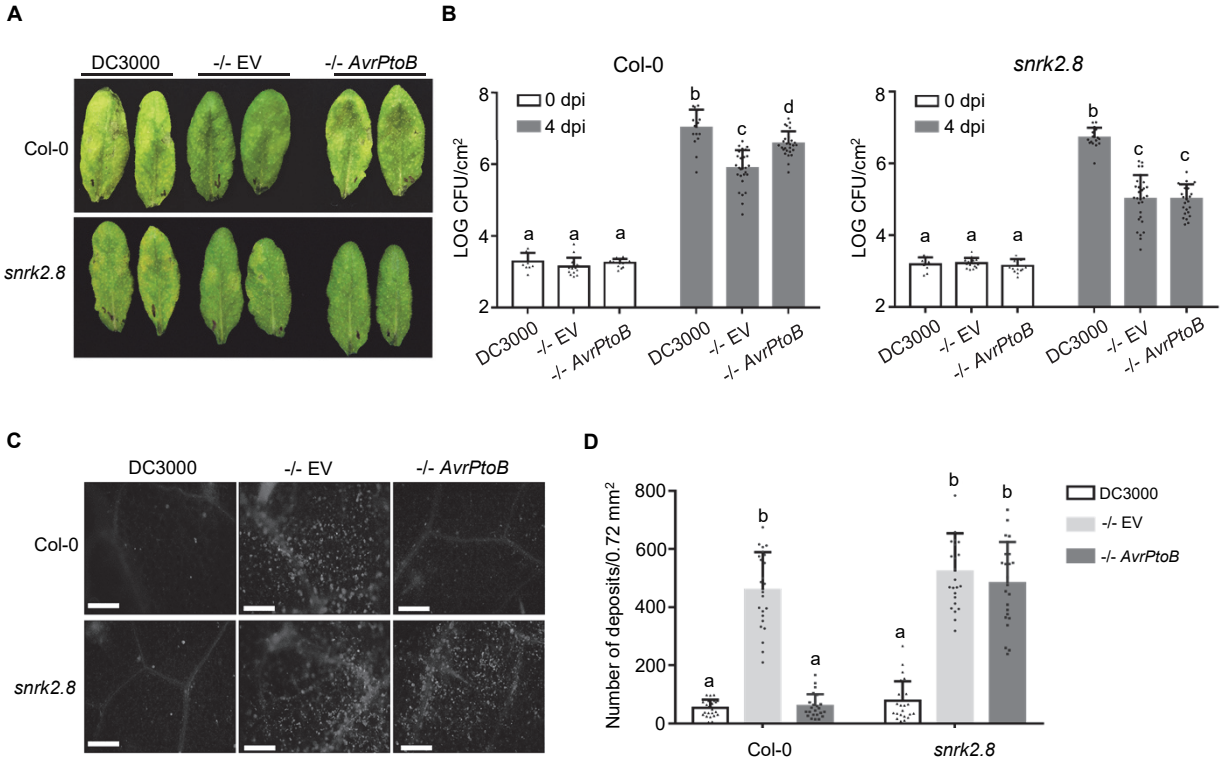

Figure 3. SnRK2.8 is required for AvrPtoB virulence.

(A) Disease symptoms of *Arabidopsis* Col-0 and the *snrk2.8* knockout after infection with *P. syringae* pv. *tomato* DC3000 (DC3000) variants. DC3000 and DC3000Δ*avrPto*Δ*avrPtoB* (-/-) carrying empty vector (EV) or expressing *AvrPtoB* on a plasmid were syringe infiltrated into *Arabidopsis* Col-0 and *snrk2.8* at a concentration of 2×10^5 CFU mL^{-1}. Disease symptoms were observed 4 days post-inoculation (dpi).
(B) Bacterial populations in Col-0 and *snrk2.8* leaves 4 dpi. Bacterial inoculations were performed as described in (A). LOG CFU/cm^2 = log colony forming units per cm^2 of leaf tissue. Data are means ± SD ($n \geq 9$ plants for day 0, $n \geq 18$ plants for day 4). Different letters indicate significant differences (two-way ANOVA, Tukey's test, $p < 0.05$).
(C) Callose deposition in *Arabidopsis* Col-0 and *snrk2.8* after inoculation with DC3000, -/- EV, and -/-*AvrPtoB*. Leaves were inoculated with *P. syringae* at a concentration of 1×10^8 CFU mL^{-1} and harvested 16h later. Leaves were stained by 1% aniline blue and imaged by fluorescence microscopy. Scale bar, 100 µm.
(D) Quantification of callose deposits. Data from three independent experiments were used for statistical analysis. Data are means ± SD (n = 24 images from 24 leaves). Different letters indicate significant differences (two-way ANOVA, Tukey's test, $p < 0.05$).

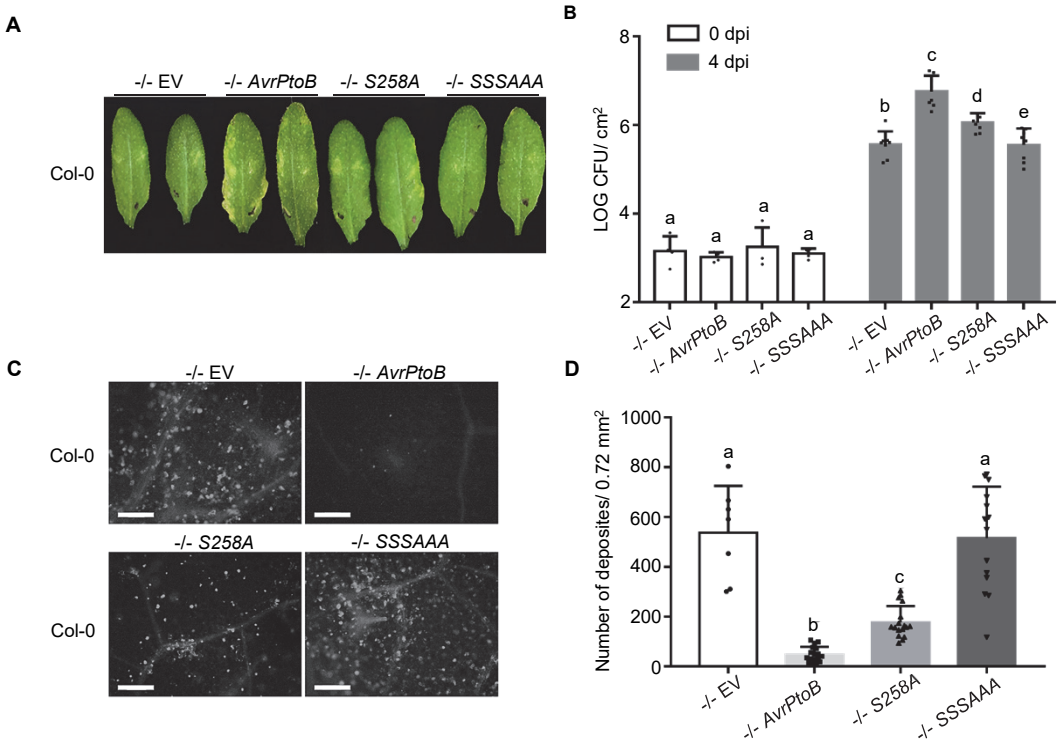

Figure 4. Phosphorylated AvrPtoB serine residues are required for virulence.

(A) Disease symptoms of *Arabidopsis* Col-0 after inoculation with *P. syringae* pv. *tomato* DC3000Δ*avrPto*Δ*avrPtoB* (-/-) variants. DC3000 -/- carrying empty vector (EV) or plasmids expressing wild-type *AvrPtoB*, $AvrPtoB_{S258A}$, or $AvrPtoB_{S205AS210AS258A}$ (*SSSAAA*) were syringe infiltrated into *Arabidopsis* Col-0 at a concentration of 2×10^5 CFU mL^{-1}. Disease symptoms were observed 4 days post-inoculation (dpi).
(B) Bacterial populations in Col-0 leaves 4 dpi. Bacterial inoculations were performed as described in (A). LOG CFU/cm^2 = log colony-forming units per cm^2 of leaf tissue. Data are means ± SD (n = 4 plants for day 0; n = 8 plants for day 4). Different letters indicate significant differences (two-way ANOVA, Tukey's test, $p < 0.05$).
(C) Callose deposition in *Arabidopsis* Col-0 after inoculation with -/- carrying EV, *AvrPtoB*, *S258A*, and *SSSAAA*. Leaves were inoculated with *P. syringae* at a concentration of 1×10^8 CFU mL^{-1} and harvested 16h later. Leaves were stained by 1% aniline blue and imaged by fluorescence microscopy. Scale bar, 100 µm.
(D) Quantification of callose deposits. Data are means ± SD (n = 8 images from 8 leaves for -/- EV, n = 18 images from 18 leaves for rest variants). Different letters indicate significant differences (one-way ANOVA, Tukey's test, $p < 0.05$).

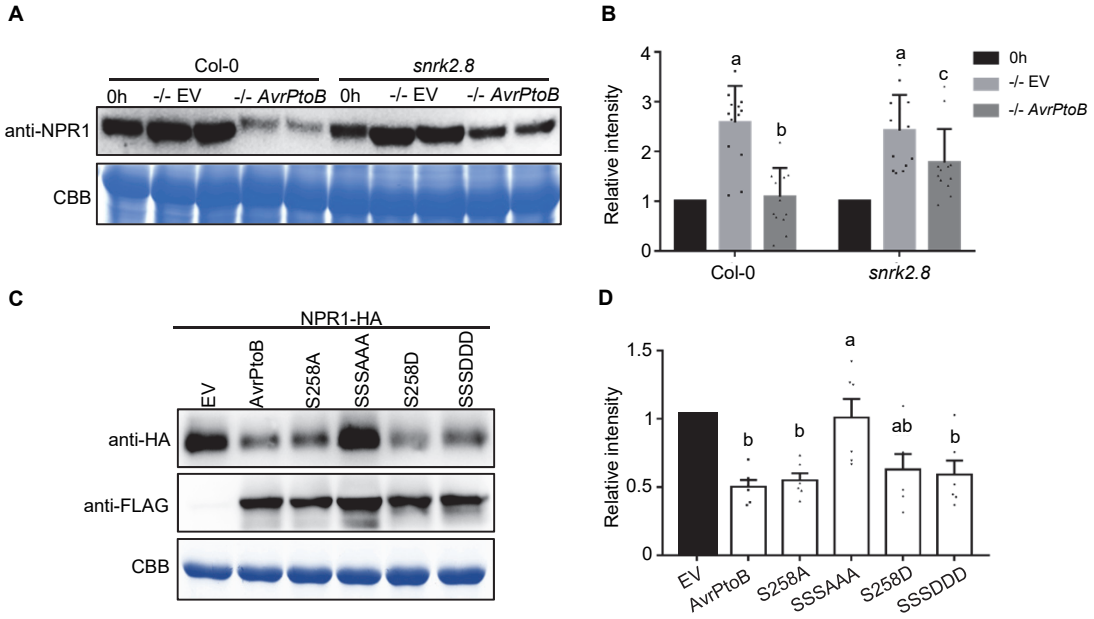

Figure 5. AvrPtoB-mediated degradation of NPR1 requires the plant kinase SnRK2.8.

(A) NPR1 accumulation in *Arabidopsis* Col-0 and the *snrk2.8* knockout after inoculation with *P. syringae* pv. *tomato* DC3000Δ*avrPto*Δ*avrPtoB* (-/-) variants. DC3000 -/- carrying the empty vector (EV) or a plasmid expressing wild-type *AvrPtoB* were syringe infiltrated into Col-0 and *snrk2.8* at a concentration of 1×10^8 CFU mL^{-1} and proteins extracted after four hours. Protein extracts were subjected to anti-NPR1 immunoblotting. Coomassie Brilliant Blue (CBB) staining shows equal protein loading.

(B) Quantification of NPR1 band intensity in (A). NPR1 bands intensities were quantified by Image Lab 6.0.1 (BIO-RAD). The values were normalized first by Rubisco bands and subsequently by the intensities of "0h" bands. Data are means ± SD (n = 14 leaves). Different letters indicate significant differences (one-way ANOVA, Tukey's test, $p < 0.05$).

(C) NPR1 accumulation in the presence of AvrPtoB phosphorylation mutants in *N. benthamiana* after Agrobacterium-mediated transient expression. *35S::NPR1-HA* was co-expressed with FLAG-tagged Dex-inducible *AvrPtoB*, $AvrPtoB_{S258A}$, $AvrPtoB_{S205AS210AS258A}$ (*SSSAAA*), $AvrPtoB_{S258D}$ or $AvrPtoB_{S205DS210DS258D}$ (*SSSDDD*). The Dex inducible EV was used as a control. The expression of AvrPtoB-FLAG phosphorylation variants was induced by 15 µM DEX for 5 hours 24h post-Agrobacterium infiltration. Protein extracts were subjected to anti-HA and anti-FLAG immunoblotting. CBB staining shows protein loading.

(D) Quantification of NPR1-HA band intensity in (C). NPR1-HA bands intensities were quantified by Image Lab 6.0.1 (BIO-RAD). The values were normalized first by Rubisco bands and subsequently by the intensities of "EV" treatment. Data are means ± SD (n = 6 leaves). Different letters indicate significant differences (one-way ANOVA, Tukey's test, $p < 0.05$).

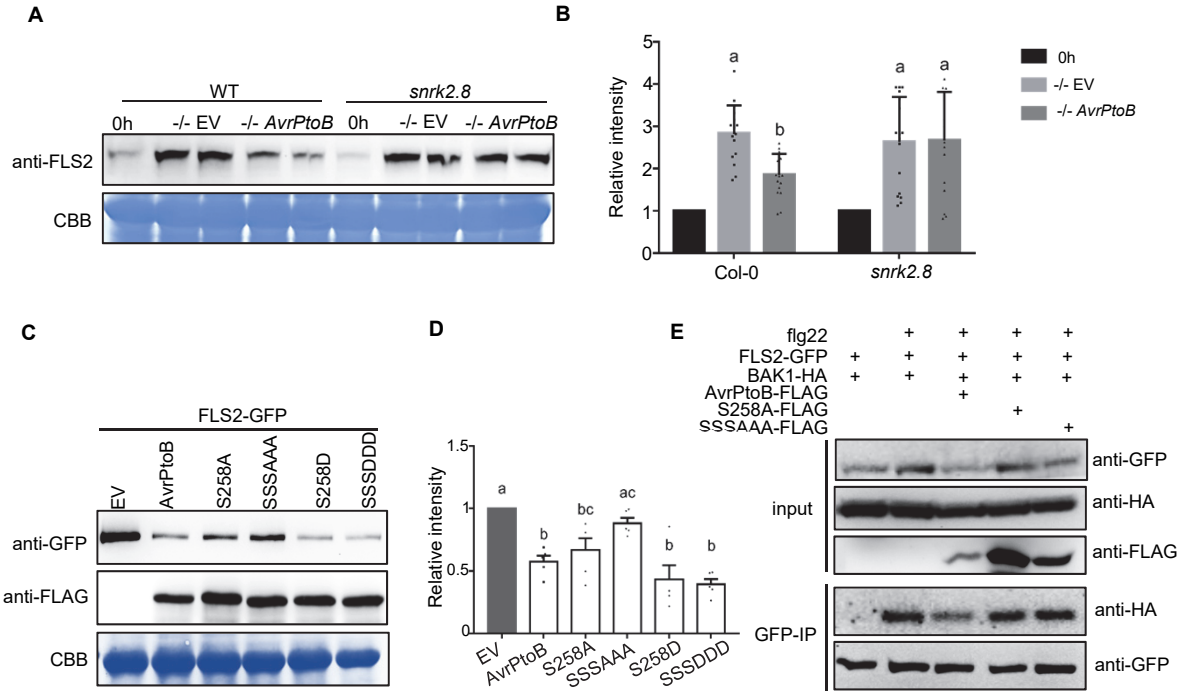

Figure 6. AvrPtoB-mediated degradation of FLS2 and inhibition of FLS2 complex formation requires the plant kinase SnrK2.8 and phosphorylated residues.

(A) FLS2 accumulation in *Arabidopsis* Col-0 and the *snrk2.8* knockout after inoculation with *P. syringae* pv. *tomato* DC3000Δ*avrPto*Δ*avrPtoB* (-/-) variants. DC3000 -/- carrying the empty vector (EV) or a plasmid expressing wild-type *AvrPtoB* were syringe infiltrated into Col-0 and *snrk2.8* at a concentration of 1×10^8 CFU mL^{-1} and proteins extracted after 8h. Protein extracts were subjected to anti-FLS2 immunoblotting. Coomassie Brilliant Blue (CBB) staining shows equal protein loading.

(B) Quantification of FLS2 band intensity in (A). FLS2 band intensities were quantified by Image Lab 6.0.1. The values were normalized first by Rubisco bands and subsequently by the intensities of "0h" bands. Data are means ± SD (n = 14 leaves). Different letters indicate significant differences (one-way ANOVA, Tukey's test, $p < 0.05$).

(C) FLS2 accumulation in the presence of AvrPtoB phosphorylation mutants in *N. benthamiana* after Agrobacterium-mediated transient expression. *35S::FLS2-GFP* was co-expressed with FLAG-tagged Dex-inducible *AvrPtoB*, $AvrPtoB_{S258A}$, $AvrPtoB_{S205AS210AS258A}$ (*SSSAAA*), $AvrPtoB_{S258D}$, or $AvrPtoB_{S205DS210DS258D}$ (*SSSDDD*). The Dex inducible EV was used as a control. The expression of AvrPtoB-FLAG phosphorylation variants was induced by 15 µM DEX for 5 hours 24h post-Agrobacterium infiltration. Protein extracts were subjected to anti-GFP and anti-FLAG immunoblotting. CBB staining shows protein loading.

(D) Quantification of FLS2-GFP band intensity in (C). FLS2-GFP bands intensities were quantified by Image Lab 6.0.1. The values were normalized first by Rubisco bands and subsequently by the intensities of "EV" treatment. The data from two independent experiments were used for statistical analysis. Data are means ± SD (n = 6 leaves). Different letters indicate significant differences (one-way ANOVA, Tukey's test, $p < 0.05$).

(E) Analyses of AvrPtoB-mediated inhibition of FLS2 complex formation. AvrPtoB-FLAG variants, BAK1-HA, and FLS2-GFP were co-expressed in the indicated combinations in *N. benthamiana* using Agrobacterium-mediated transient expression. The expression of AvrPtoB-FLAG phosphorylation variants was induced by 15 µM DEX for 3 hours 24h post-Agrobacterium infiltration. Leaves were infiltrated with 10 µM flg22 peptide 15 minutes before harvesting protein extracts for GFP immunoprecipitation and western blotting. Protein inputs and immunoprecipitated samples were detected by immunoblot.